

Article

Biocompatible Organic Coatings Based on Bisphosphonic Acid RGD-Derivatives for PEO-Modified Titanium Implants

Lyudmila V. Parfenova ^{1,*} , Elena S. Lukina ¹, Zulfia R. Galimshina ¹, Guzel U. Gil'fanova ¹, Veta R. Mukaeva ², Ruzil G. Farrakhov ², Ksenia V. Danilko ³, Grigory S. Dyakonov ⁴ and Evgeny V. Parfenov ² 

¹ Institute of Petrochemistry and Catalysis of Russian Academy of Sciences, 141, Prospekt Oktyabrya, 450075 Ufa, Russia; elenlykina@mail.ru (E.S.L.); zgalimshina@mail.ru (Z.R.G.); gilfanova.guzel@gmail.com (G.U.G.)

² Department of Theoretical Basis of Electrical Engineering, Ufa State Aviation Technical University, 12 Karl Marx Street, 450008 Ufa, Russia; veta_mr@mail.ru (V.R.M.); frg1982@mail.ru (R.G.F.); evparfenov@mail.ru (E.V.P.)

³ Bashkir State Medical University, 3 Lenin Street, 450000 Ufa, Russia; kse-danilko@yandex.ru

⁴ Institute of Physics of Advanced Materials, Ufa State Aviation Technical University, 12 Karl Marx Street, 450008 Ufa, Russia; dgr84@mail.ru

* Correspondence: luda_parfenova@ipc-ras.ru; Tel.: +7-347-284-3527

Academic Editor: Derek J. McPhee

Received: 26 November 2019; Accepted: 1 January 2020; Published: 6 January 2020



Abstract: Currently, significant attention is attracted to the problem of the development of the specific architecture and composition of the surface layer in order to control the biocompatibility of implants made of titanium and its alloys. The titanium surface properties can be tuned both by creating an inorganic sublayer with the desired morphology and by organic top coating contributing to bioactivity. In this work, we developed a composite biologically active coatings based on hybrid molecules obtained by chemical cross-linking of amino acid bisphosphonates with a linear tripeptide RGD, in combination with inorganic porous sublayer created on titanium by plasma electrolytic oxidation (PEO). After the addition of organic molecules, the PEO coated surface gets nobler, but corrosion currents increase. In vitro studies on proliferation and viability of fibroblasts, mesenchymal stem cells and osteoblast-like cells showed the significant dependence of the molecule bioactivity on the structure of bisphosphonate anchor and the linker. Several RGD-modified bisphosphonates of β -alanine, γ -aminobutyric and ϵ -aminocaproic acids with BMPS or SMCC linkers can be recommended as promising candidates for further in vivo research.

Keywords: titanium implants; plasma electrolytic oxidation; RGD peptide; bisphosphonic acid; in vitro tests; fibroblasts; mesenchymal stem cells; human osteosarcoma cells

1. Introduction

Traumatology and orthopedics generate high demand in implants for osseosynthesis, and, according to market forecasts, this demand will increase due to the spread of extreme activities and the aging of the population. Currently, various biomimetic approaches that ensure the biocompatibility of the implants are developed [1]. As a rule, they suggest changes in the architecture and composition of the surface layer so that the devices gain the properties of the bone tissue and cell membranes. In current medical practice, preference is given to implants made of titanium and its alloys, due to their bioinert properties and high corrosion resistance [2]. The modification of the titanium surface is achieved both through inorganic coatings that approximate the phase composition and morphology of

the human bone and by introduction of organic molecules containing functional fragments actively interacting with the proteins of the extracellular matrix (ECM). These approaches should provide both biomechanical and biochemical compatibility of the implants, their corrosion resistance, and, therefore, should successfully initiate the metal device osseointegration into the bone tissue.

Currently, significant attention is attracted to the biomimetic coatings based on the method of plasma electrolytic oxidation (PEO) [3,4]. The inorganic parts of the PEO coatings contain stable titania (rutile and anatase) tightly attached to the surface [5]. PEO helps to incorporate the anions and cations of the electrolyte into the coating; this provides Ca-, P- containing bioactive crystalline phases within the coating: hydroxyapatite, tricalciumphosphate, tetracalciumphosphate, perovskite [6]. Nevertheless, medical implants, once introduced into a biological system, get covered by nonspecific proteins within a few seconds. The adsorbed layer initiates a foreign body reaction of the organism; this causes the formation of a vascular fibrous capsule isolating the implant from the target tissue [7]. Consequently, current state-of-the-art includes the development of biocompatible bifunctional organic top coatings, which, on one hand would mask the implant, on the other hand, would initiate the implant osseointegration. These modern materials include: non-fouling coatings based on polysaccharides; hydrophilic self-assembled monolayers or polyethylene glycol, also in combination with oligopeptides (OP); bioactive coatings based on the extracellular matrix proteins (e.g., fibronectin, collagen, laminin, and osteopontin), having both long and short sequences of the amino acids [8–12]. The combination of the PEO inorganic sublayer and the organic top coating appears to be a promising direction for the development of implants with enhanced osseointegration [13–15].

Among relatively short bioactive peptide sequences, special attention is paid to RGD (arginine-glycine-aspartic acid), which is a tripeptide fragment appearing in numerous extracellular matrix proteins, and to which the cells attach using specific receptors on their surface [16]. Its discovery led to the identification of a large family of the cell surface adhesion receptors, called integrins, which recognize RGD-specific sequences in certain proteins of the extracellular matrix. The literature survey shows significant research efforts put into the application of the RGD-containing oligopeptides for the titanium surface modification. Various methods of the deposition have been developed: silanization of the surface by aminosilanes (including APTES) followed by the binding with RGD-containing oligopeptide via various linkers [17–30]; oligopeptide- functionalized synthetic polymers [31–34] and natural biopolymers [35–39]; oligopeptides attachment to the titanium via CDI [40,41] or tresyl chloride [42] surface activation; immobilization of OP on Ti via electrodeposited poly(ethyleneglycol) (PEG) [43–45]; physicochemical adsorption of oligopeptides as well as SH-ended derivatives [23,46–51] and 3,4-dihydroxyphenylalanine (DOPA) functionalized OP [52] from solutions; physicochemical adsorption of OP with a phosphonate anchor [22,23,36,51,53–58]. The strategy of the phosphonate anchors appears to be very attractive when bonding the inorganic oxide sublayer with the organic top coating. As shown elsewhere [59–61], phosphonate groups have high affinity to metal ions and their oxides, and they are almost not prone to hydrolytic cleavage, unlike siloxanes [62,63]. The introduction of gem-bisphosphonic group into the molecules increases their affinity to the oxidized surfaces compared to monophosphonates, and this increases their aqueous solubility due to the changing of the molecule polarity [64,65].

Plasma electrolytic oxidation currently is a well-developed electrochemical technique used to produce ceramic coatings with improved adhesion over the surface of valve metals such as titanium, magnesium, aluminum and zirconium [66–68]. Due to the unique surface morphology of the porous coating, PEO provides better biocompatibility of the surface and for the cell proliferation [69]. The PEO process is an expansion of the traditional anodizing into high voltages of up to 600 V; these voltages promote microdischarges within the coating; this results in its resolidifying and intensive growth [70]. The process mechanism includes electrochemical oxidation and numerous melting and crystallizing events at the microdischarge sites. This coating formation mechanism helps to develop coatings with regulated porosity, with the pore size from 0.1 to 10 μm and roughness R_a from 1 to 10 μm ; the wide network of the pores forms a fractal-like structure, with the pore size increasing to the top of the

coating [71]. The high surface area of the PEO coating allows deposition of various functional organic components, and the PEO coating acts as a sublayer increasing adhesion, and as the organic substance carrier [72–76].

Our recent study [15] showed that the combination of the PEO coating and RGD-modified bisphosphonic acid on nano-Ti gives a 45% increase in the number of proliferated cells compared to uncoated nano-Ti, and 66% compared to coarse grain Ti.

In the presented study, we expanded the number of hybrid RGD-functionalized molecules in order to understand how the structure of the bisphosphonate anchors and linkers (BMPS, EMCS, SMCC) affects the biological activity of the composite coatings based on inorganic porous PEO sublayer on titanium; moreover, the biological effect of the synthesized organic molecules was studied in vitro on a larger set of cell lines (mesenchymal stem cells, fibroblasts and osteoblast-like cells). Therefore, the aim of this work is to synthesize the hybrid molecules by chemical cross-linking of amino acid bisphosphonates with a linear RGD tripeptide through linkers that differ in length and structure for effective use in combination with inorganic porous PEO sublayer on titanium, and to identify the most promising options for the design of the proposed biomimetic coatings.

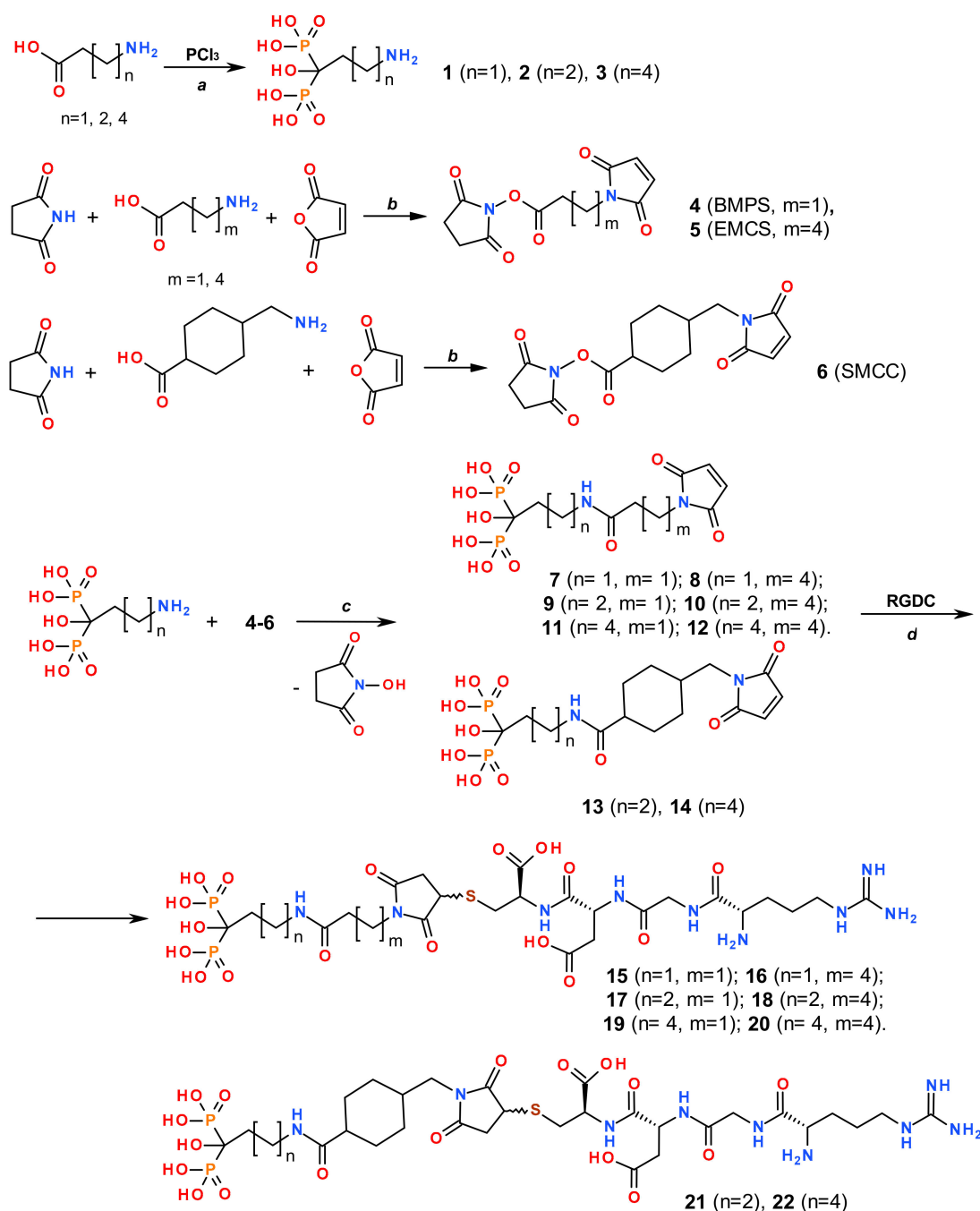
2. Results and Discussion

The experimental design concerns the variation of the anchors and linkers to attach the RGD peptide to the titanium implant. For the sake of the clarity, the following sample identification is used: Ti—for the metal substrate; Ti-PEO—for the inorganic PEO coating over the substrate; Ti-PEO-RGD—for the PEO coating soaked in the RGD aqueous solution; Ti-PEO-(number)-RGD—for the PEO coating soaked in the aqueous solution of the RGD-modified bisphosphonic acids, where the (number) indicates the compound in accordance with the reaction Scheme 1 and the corresponding description in Section 3.2. As a result, this sample identification shows the structures of the proposed composite coatings.

2.1. Synthesis of Bioactive Bifunctional Molecules

As a base for the design of the RGD-containing self-assembled monolayers on the PEO-modified metal surface, we synthesized amino acid bisphosphonates 1–3 via the reaction of the corresponding amino acids (β -alanine, γ -aminobutyric and ϵ -aminocaproic acids) with PCl_3 in methanesulfonic acid (Scheme 1). We found that carrying out the synthesis at elevated temperature (85–90 °C) decreases the reaction time to 4–5 h, and, along with the separation of the products at pH = 6, increases the resulting yield of the amino bisphosphonates up to 85–89%. The *N*-maleimidosuccinimide linkers (BMPS, EMCS and SMCC) 4–6 were obtained in yields of 60–89% via the reaction of maleic anhydride, *N*-hydroxysuccinimide and aminocarboxylic acids in DMF [77,78]. The *N*-maleimido derivatives 7–14 for further modification by the oligopeptide were obtained by interaction of amino bisphosphonates with *N*-maleimidosuccinimide linkers. The application of acetone instead of dioxane as the solvent used elsewhere [79] helped to avoid the formation of relatively heavy side products whose appearance is an inevitable consequence of the dioxane cycle modification. Target RGD-modified amino acid bisphosphonates 15–22 were obtained by the reaction of the corresponding derivatives 7–14 with RGDC in an aqueous medium at pH = 7 by Michael reaction.

The structure of the RGD-modified amino acid bisphosphonates was confirmed by mass-spectrometry MALDI TOF/TOF, 1D (^1H , ^{13}C , ^{31}P) and 2D NMR spectroscopy. In the MALDI TOF/TOF mass spectra of the hybrid molecules, the peaks with m/z corresponding to the molecular ions were detected. The ^{31}P -NMR spectra exhibited single resonance lines at δ_{P} 17–18 ppm, characteristic to bisphosphonate groups. Signals corresponding to fragments of amino bisphosphonate, linker, and RGDC were observed in ^1H - and ^{13}C -NMR spectra. The formation of compounds 15–22 was accompanied by the disappearance of the signal of double bond protons of the *N*-maleimido fragment in derivatives 7–14 at δ_{H} 6–7 ppm in the ^1H -NMR spectrum.



Scheme 1. Reagents and conditions: (a) MeSO_3H , 4–5 h, 85–90 °C; (b) DMF, 3–16 h, 0–25 °C; (c) H_2O : acetone = 1:1, pH = 8–9, 1 h, 38–40 °C; (d) H_2O , pH = 7, 1–1.5 h, 38–40 °C.

2.2. PEO Coating Characterization

Figure 1 shows the top view and cross-section of the PEO coating. The coating exhibits a porous morphology, with porosity evaluated as $18.2 \pm 2.5\%$. The coating thickness is $19.3 \pm 1.5 \mu\text{m}$, surface roughness $1.5 \pm 0.2 \mu\text{m}$. This type of morphology contributes towards cell proliferation, and it supplies a well-developed surface for the introduction of the organic compounds with bisphosphonate anchors into the resulting composite coating [15]. The coating surface porosity is $9.5 \pm 0.8\%$; the real 3D structure of this well-developed network of pores can be seen elsewhere for a similar PEO coating [80].

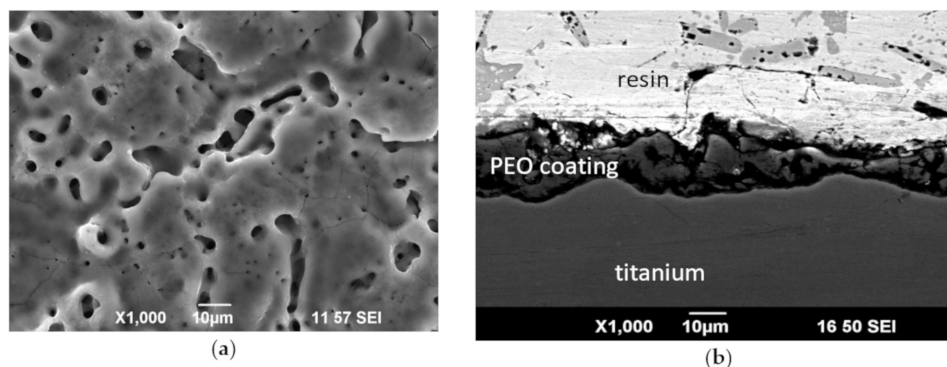


Figure 1. SEM images of the PEO coating: (a) Top view; (b) Cross-section.

As follows from Figure 2, the PEO coating consists of crystalline titania in two phase modifications—rutile and anatase (49 and 51% respectively). Also, the XRD pattern shows the peaks belonging to α -Ti substrate. This coating composition and morphology provides sufficient surface passivation for the implant prolonged operation in the corrosive fluids of a human body [81]. Also, this type of coating exhibits exceptional adhesion to the titanium surface as summarized elsewhere [5].

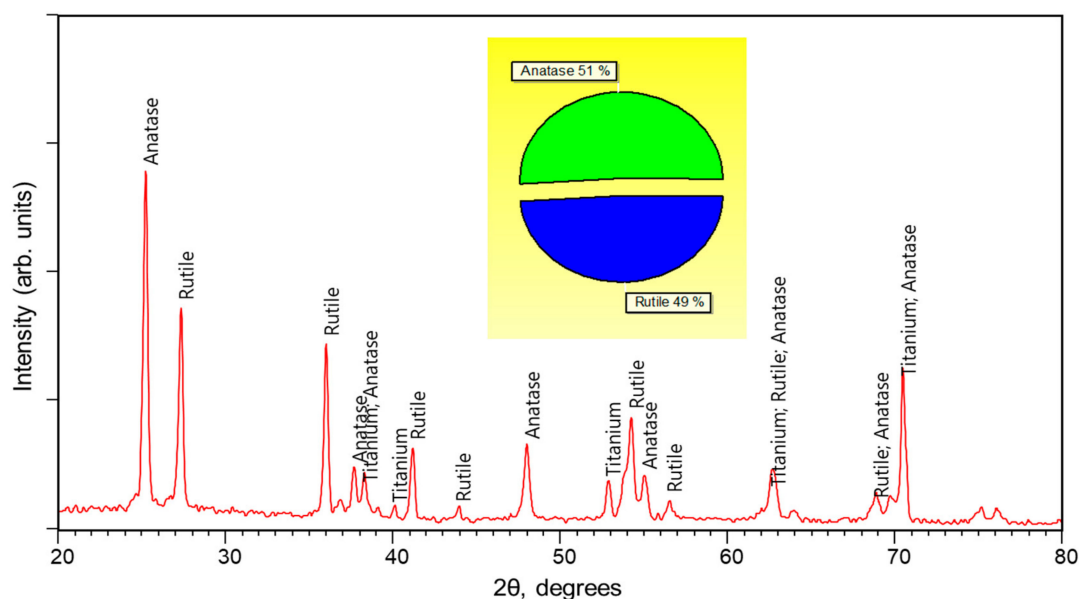


Figure 2. XRD pattern of the PEO coating with the labeled peaks and SemiQuant results.

2.3. XPS Analysis of the Composite PEO Coating Functionalized with RGD Derivatives

Since the introduction of the RGD derivatives into the inorganic PEO coating was performed at a low concentration of 10^{-3} M, it falls below the capabilities of the SEM and XRD techniques to detect organic compounds on the titania surface. Therefore, XPS studies were employed in order to verify the presence of the RGD derivatives within the coating; a typical survey spectrum is shown in Figure 3. In details the XPS spectra are presented in the Supplementary Materials. The survey XPS spectra collected from the PEO-coated titanium samples indicate typical Ti 2p, Ti 3s O 1s, C 1s, P 2p, N 1s, O KLL and Ti LMM Auger peaks. The spectra of the RGD-modified samples confirm changes in the surface layer chemistry compared to the unmodified PEO sample.

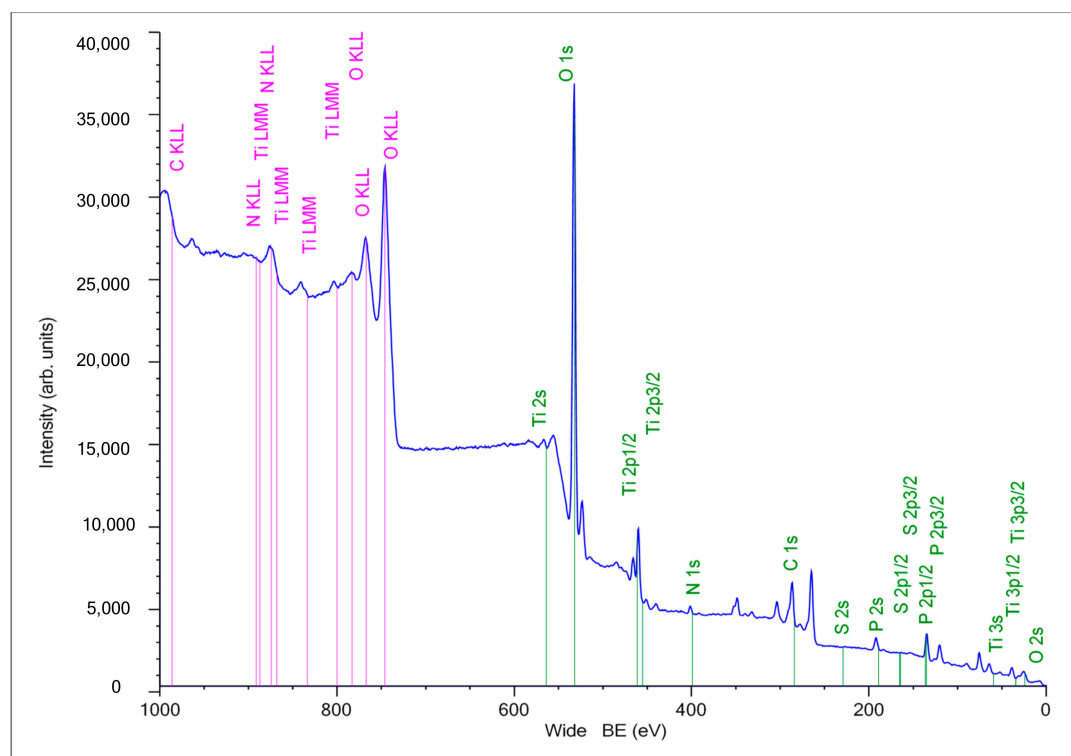


Figure 3. Survey XPS spectra of the Ti-PEO coating.

As follows from the high-resolution XPS spectra, the organic molecules attached to the surface affect the relative content of nitrogen, phosphorus, carbon, oxygen, and sulfur (Table 1). The most notable differences appear for the Ti2p, C1s and N1s peaks. The Ti2p signal decreased after the RGD modification, and the N1s and C1s signals increased. Also, the RGD-modified surface shows the presence of S2p signals, whereas for the Ti-PEO surface this signal does not appear. The changes in the atomic ratio (Ti2p/C1s) and (Ti2p/P2p) show that the titanium signal decreases for all the RGD modified types of the surface. This is consistent with the observations made elsewhere [27,82,83].

Table 1. Atomic composition and atomic ratio derived from XPS high-resolution spectra for the Ti-PEO samples with and without RGD modification.

Sample	XPS Atomic Composition (at %)						Atomic Ratio	
	N1s	P2p	C1s	O1s	Ti2p	S2p	Ti2p/C1s	Ti2p/P2p
Ti-PEO	1.48	3.57	7.00	70.49	17.36	0.00	2.48	4.86
Ti-PEO-15-RGD	5.43	6.96	13.34	67.25	6.72	0.30	0.50	0.97
Ti-PEO-16-RGD	4.87	4.60	13.54	60.59	16.39	0.00	1.21	3.56
Ti-PEO-17-RGD	2.37	6.06	15.48	65.20	10.79	0.00	0.70	1.78
Ti-PEO-18-RGD	5.86	3.01	25.92	57.20	7.50	0.50	0.29	2.49
Ti-PEO-19-RGD	2.88	3.52	14.32	67.96	11.10	0.21	0.78	3.15
Ti-PEO-20-RGD	2.35	6.00	18.03	67.36	6.27	0.00	0.35	1.05

2.4. Electrochemical Behavior of the Composite PEO Coating Functionalized with RGD Derivatives

The electrochemical behavior of the composite PEO coating functionalized with RGD derivatives was studied using compounds 15–18 as examples. The polarization curves (Figure 4) show notable differences among the surface having PEO and various RGD treatments. As expected, after the PEO, the surface passivates, and the E_{corr} becomes nobler; the corrosion current i_{corr} decreases, which is followed by an order of magnitude increase in the polarization resistance R_p (Figure 5). All the RGD functionalized coatings show the surface, nobler than that of the Ti-PEO sample. The cathodic parts of the polarization curves do not show significant differences compared to Ti and Ti-PEO samples. This indicates that cathodic corrosion processes are not influenced by this type of coating since the cathodic

Tafel parts show almost similar slopes. However, the anodic behavior is significantly influenced by the coating. Ti-PEO sample shows a passivation region above -0.1 V(AgCl). The introduction of the RGD-modified bisphosphonates depassivates the surface; the corrosion current increases compared to that of Ti-PEO and Ti samples (Figure 5). The depassivation region belongs to the range -0.1 to 0.1 V (AgCl) and ends with a pitting current tip followed by a passivation region above 0.1 V (AgCl). The changes in the anodic kinetics rise the E_{corr} , and this is followed by the increase of the i_{corr} . This indicates that the RGD functionalization increases the exchange currents, and this i_{corr} behavior is supported by the decrease of R_p .

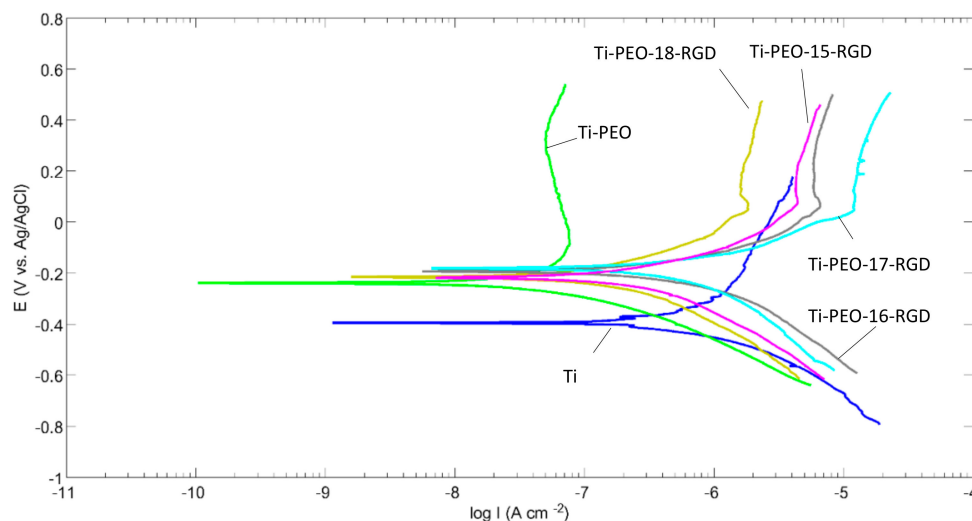


Figure 4. Polarization curves in Ringer's solution for the Ti samples, with PEO coating, and RGD modification.

2.5. In Vitro Test Results Supporting The Efficiency of Proposed PEO Coating Functionalized with RGD Derivatives

As follows from the literature analysis, the application of RGD-containing bisphosphonates to the titanium surface leads to the increase in cell adhesion, proliferation and mineralization [22,23,51,53]. The cell adhesion appeared to be sensitive to the anchor used [57,59].

The in vitro results presented in Figure 6 show that the different cell lines give dissimilar reactions to the same type of coating. The biological response also depends on the structure of the source amino bisphosphonate and the linker. It was shown that RGDC-oligopeptide itself introduced into the PEO coating without the anchor does not affect the cell life activity on the surface.

A significant (up to 30–40%) increase in the fibroblast proliferation was observed when using the organic molecules with relatively short linkers and aminobisphosphonate fragments BMPS- β (Ti-PEO-15-RGD) and BMPS- γ (Ti-PEO-17-RGD). Moreover, the sample Ti-PEO-15-RGD based on β -alanine bisphosphonate with the short BMPS linker and RGD peptide has shown the best adhesion for the osteoblast-like cells MG-63 compared to the other samples.

The derivatives containing EMCS linker (Ti-PEO-16-RGD and Ti-PEO-18-RGD) lead to a decrease in the proliferation of MG-63 on the PEO-modified surface. The same tendency was found in the case of mesenchymal stem cells then the long-chained molecules containing EMCS linker (Ti-PEO-16-RGD, Ti-PEO-18-RGD, and Ti-PEO-20-RGD) or derivative of ϵ -aminocaproic acid (Ti-PEO-19-RGD) were applied. In contrast, SMCC-linked compounds (Ti-PEO-21-RGD and Ti-PEO-22-RGD) provide the increasing of the cell growth up to 20% on the surface.

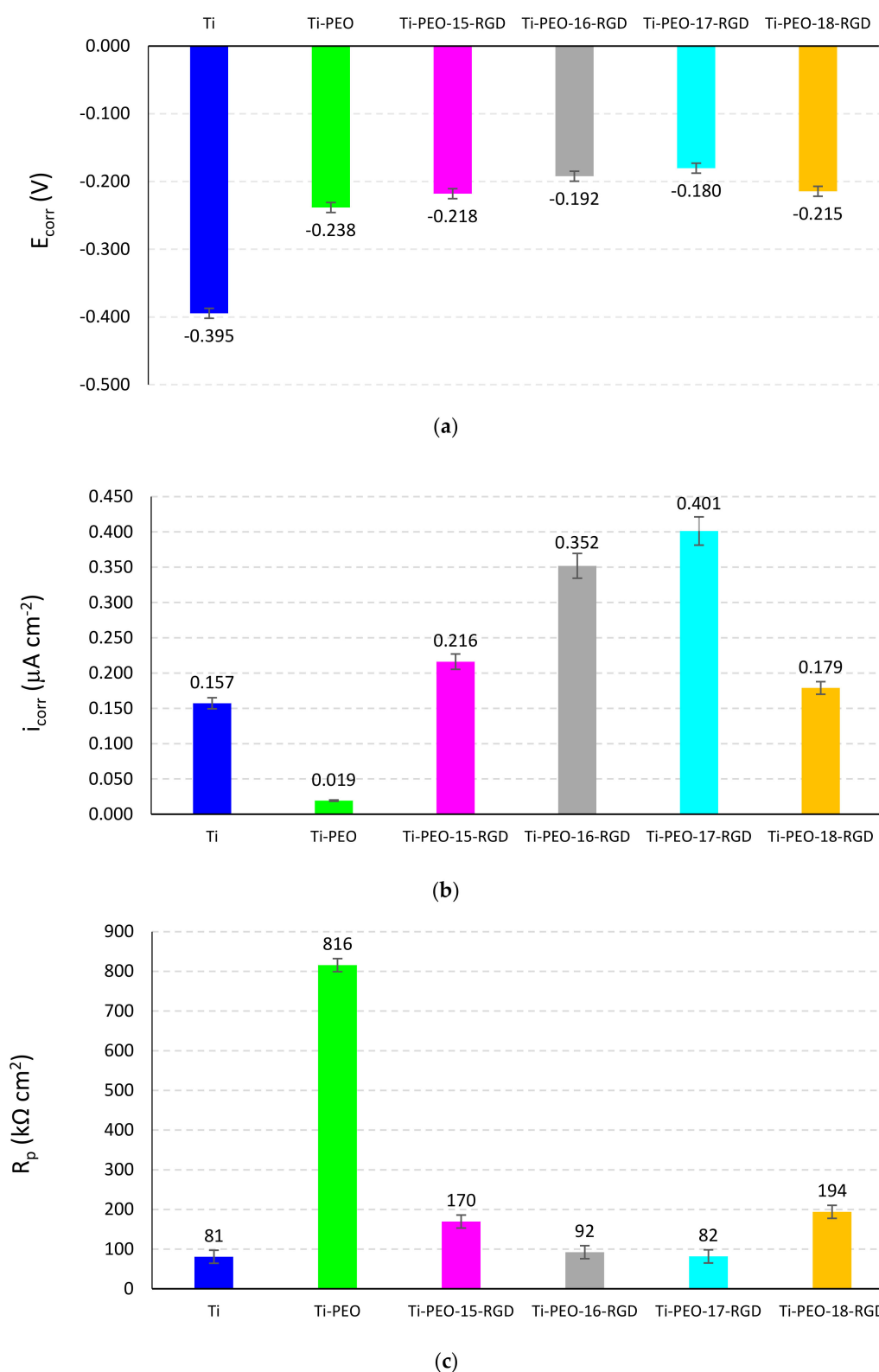


Figure 5. Electrochemical properties in Ringer's solution for the Ti samples, with PEO coating, and RGD modification: (a) Corrosion potential E_{corr} ; (b) Corrosion current i_{corr} ; (c) Polarization resistance R_p .

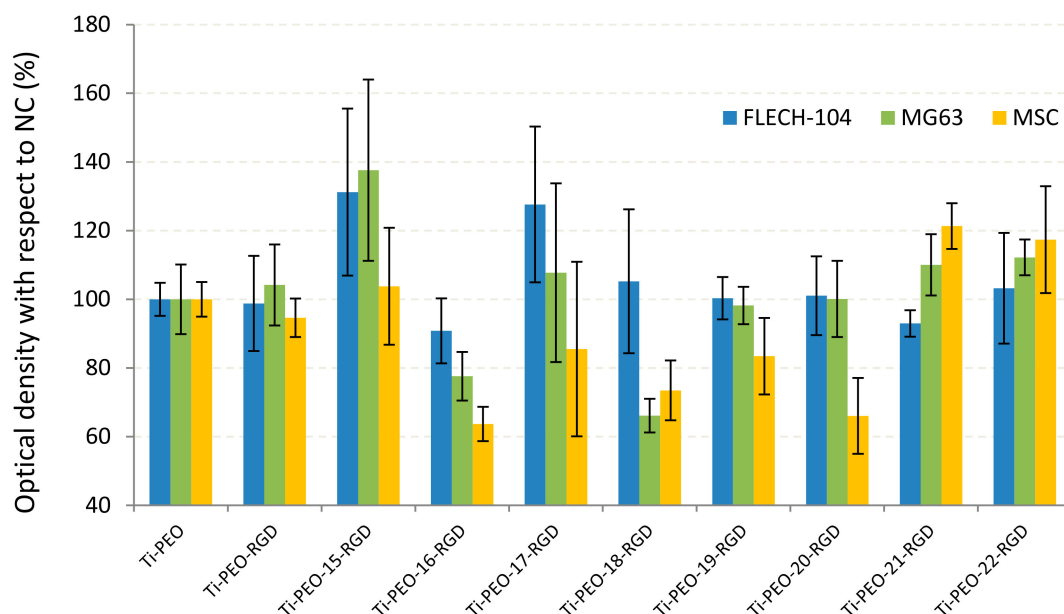


Figure 6. Optical density showing viability and proliferation of fibroblasts (FLECH-104), human osteoblast-like cells (MG-63) and mesenchymal stem cells (MSC) cultured on the surface of Ti-PEO functionalized by RGD-derivatives (15–22) after 7 days (metal samples were kept for 1 h at room temperature in the solutions of compounds 15–22 with concentrations 1.3×10^{-3} – 1.8×10^{-3} M/L and then dried).

Summarizing the *in vitro* studies, we can conclude that RGD functionalized hybrid molecules **15**, **17**, **21**, **22** appear to be promising organic top coatings for modulation of the biological activity of the PEO modified surface of titanium implants. The differences in the cell behavior depending on the compound structure can be caused by their cytotoxicity and orientation on the PEO surface during adsorption; this requires further studies that are currently conducted in our research group.

3. Materials and Methods

3.1. General Information

The following reagents were used for the synthesis: methanesulfonic acid (98%, Acros Organics, Geel, Belgium), PCl_3 (98%, Acros Organics), β -alanine (97%, Acros Organics), γ -aminobutanoic (99+%, Acros Organics) and ϵ -aminocaproic acid ($\geq 98.5\%$, Merck, Darmstadt, Germany), maleic anhydride (98+%, Acros Organics), *N*-hydroxysuccinimide (98+%, Acros Organics), dicyclohexylcarbodiimide (DCC, 99%, Acros Organics) and RGDC oligopeptide (Arg-Gly-Asp-Cys trifluoroacetate, Bachem, Bubendorf, Switzerland).

Spectroscopic studies were performed by ^1H , ^{13}C and ^{31}P -NMR on an AVANCE-500 spectrometer (Bruker, Rheinstetten, Germany; operating frequency 500.17 MHz (^1H), 125.78 MHz (^{13}C) and 202.48 MHz (^{31}P)). D_2O and CDCl_3 were used as internal standards and solvents. ^{31}P -NMR chemical shifts are given relative to the standard, an 85% solution of H_3PO_4 in H_2O (δ_{P} 0 ppm). Samples were prepared in a standard tube with a diameter of 5 mm. The chemical shifts of carbon and hydrogen atoms are given on the scale δ (ppm) with respect to TMS, the KCCB values (J) are given in Hz. One and two-dimensional NMR spectra (COSY HH, HSQC, HMBC, NOESY) were recorded using standard pulse sequences. Mass spectra were obtained on MALDI-TOF/TOF Autoflex III system (Bruker) using 2,5-dihydroxybenzoic acid (2,5-DHB) or α -cyano-4-hydroxycinnamic acid (CHCA) as matrices.

3.2. Synthesis of RGD-Functionalized Derivatives

3.2.1. Synthesis of Amino-1-hydroxyalkan-1,1-diyl-bisphosphonic acids 1–3

The synthesis of aminobisphosphonic acids was based on a literature method [84] somewhat modified by us. A portion of the amino acid (0.025 mol) (β -alanine, γ -butanoic acid, ϵ -aminocaproic acid) is dissolved in 10 mL of methanesulfonic acid (MSA) in a flask with intensive stirring. Then, 7.0 mL (0.080 mol) of phosphorus (III) chloride is slowly added dropwise to the solution over 15 min. The contents of the flask are stirred under heating (80–85 °C) for 4–6 h, then cooled to room temperature. After cooling, 12 mL (0.67 mol) of water are added, and the reaction mixture is hydrolyzed at 105 °C for 4 h. After cooling, the pH of the solution is adjusted to 6–7 by adding to the mixture 12 mL of 50% aqueous sodium hydroxide solution. Then the reaction mass precipitated with 40 mL of MeOH. The precipitate is separated on the Schott filter. The crude product is dissolved in 20 mL of water, stirred at 50–70 °C for 30 min, then cooled and precipitated with 40 mL of MeOH. The solid phase is separated using a Schott filter.

(3-Amino-1-hydroxypropane-1,1-diyl)-bisphosphonic acid (1). Yield 5.3 g (85%). IR (ν , cm^{-1}): 3448, 1613 (OH), 1526, 916 (NH_2), 1377, 1171 (P=O), 2726, 2675, 1281 (CH_2). $^1\text{H-NMR}$ (D_2O) δ : 2.18 (sept, $^3J = 6.1$ Hz, 2H, C^2H_2), 3.24 (t, $^3J = 6.5$ Hz, 2H, C^3H_2). $^{13}\text{C-NMR}$ (D_2O) δ : 30.52 (C^2), 36.12 (C^3), 72.64 (t, $^1J_{\text{C-P}} = 133.8$ Hz, C^1). $^{31}\text{P-NMR}$ (D_2O) δ : 17.04. MALDI-TOF/TOF m/z 234.018 [$\text{M} - \text{H}$] $^+$, calc. for $\text{C}_3\text{H}_{10}\text{NO}_7\text{P}_2$ 235.069.

(4-Amino-1-hydroxybutane-1,1-diyl)-bisphosphonic acid (2). Yield 5.5 g (88%). IR (ν , cm^{-1}): 3460, 1651 (OH), 1538, 907 (NH_2), 1376, 1149 (P=O), 2526, 2435, 1272 (CH_2). $^1\text{H-NMR}$ (D_2O) δ : 1.77–1.94 (m, 4H, C^2H_2 , C^3H_2), 2.82 (t, $^3J = 6.1$ Hz, 2H, C^4H_2). $^{13}\text{C-NMR}$ (D_2O) δ : 31.90 (C^2), 23.93 (t, $^3J_{\text{C-P}} = 5.5$ Hz, C^3), 40.56 (C^4), 73.3 (t, $^1J_{\text{C-P}} = 134.1$ Hz, C^1). $^{31}\text{P-NMR}$ (D_2O) δ : 17.93. MALDI TOF/TOF m/z : 247.086 [$\text{M} - 2\text{H}$] $^+$, 269.069 [$\text{M} - 2\text{H} + \text{Na}$] $^+$, 285.036 [$\text{M} - 2\text{H} + \text{K}$] $^+$, calc. for $\text{C}_4\text{H}_{13}\text{NO}_7\text{P}_2$ 249.016.

(6-Amino-1-hydroxyhexane-1,1-diyl)-bisphosphonic acid (3). Yield 6.2 g (89%). IR (ν , cm^{-1}): 3433, 1636 (OH), 1547, 910 (NH_2), 1376, 1167 (P=O), 2723, 2671, 1282 (CH_2). $^1\text{H-NMR}$ (D_2O) δ : 1.76–1.89 (m, 2H, C^2H_2), 1.63 (quint., $^3J = 7.3$ Hz, 2H, C^5H_2), 1.33 (quint., $^3J = 7.3$ Hz, 2H, C^4H_2), 1.47–1.58 (m, 2H, C^3H_2), 2.94 (t, $^3J = 7.3$ Hz, 2H, C^6H_2). $^{13}\text{C-NMR}$ (D_2O) δ : 22.87 (t, $^3J_{\text{C-P}} = 5.6$ Hz, C^3), 26.17 (C^4), 26.33 (C^5), 33.35 (C^2), 39.27 (C^6), 74.07 (t, $^1J_{\text{C-P}} = 134.7$ Hz, C^1). $^{31}\text{P-NMR}$ (D_2O) δ : 18.48. MALDI TOF/TOF, m/z : 299.193 [$\text{M} - \text{H} + \text{Na}$] $^+$, calc. for $\text{C}_6\text{H}_{17}\text{NO}_7\text{P}_2$ 277.048.

3.2.2. Synthesis of (N-Maleimidoalkyl)succinimide Esters (4–6)

The synthesis of compounds was carried out according to the method described in [77,78]. A portion of 3 mmol of an amino acid is added to a solution of maleic anhydride (0.3 g, 3 mmol) in 4 mL of DMF, stirred for 2 h at room temperature. After complete dissolution, at a temperature of 0 °C, 0.43 g (3.75 mmol) of *N*-hydroxysuccinimide (NHS) and 1.24 g (6 mmol) of dicyclohexylcarbodiimide (DCC) are added to the solution. The reaction mass is stirred in an ice bath 5–10 min and then incubated at room temperature for a day. The formation of a white precipitate of dicyclohexylurea is observed. The precipitate is washed with 20 mL of water and 20 mL of methylene chloride. The organic layer is treated with 10 mL of water, extracted with methylene chloride, then 10 mL of 5% NaHCO_3 are added and extracted with methylene chloride (the procedure is carried out three times). The organic layer was dried over Na_2SO_4 , the solution was filtered and the solvent was evaporated at the reduced pressure. The residue was purified by column chromatography on SiO_2 with $\text{CHCl}_3/\text{MeOH}$ (from 1:0 to 100:1) as an eluent to give compounds 4–6.

(2,5-Dioxypyrrolidin-1-yl)-3-(2,5-dioxypyrrrol-1-yl)propanoate (BMPS) (4). Yield 0.47 g (60%). $^1\text{H-NMR}$ spectrum matches the one reported in [85]. $^1\text{H-NMR}$ (CDCl_3) δ : 2.84 (s, 4H, NHS), 3.04 (t, $J = 6.5$ Hz, 2H, $\text{CH}_2\text{C}=\text{O}$), 3.85 (t, $J = 6.5$ Hz, 2H, CH_2N), 6.79 (s, 2H, $\text{CH}=\text{CH}$).

(2,5-Dioxopyrrolidin-1-yl)-6-(2,5-dioxopyrrol-1-yl)hexanoate (EMCS) (5). Yield 0.55 g (60%). The $^1\text{H-NMR}$ spectrum corresponds to the one reported in [86] $^1\text{H-NMR}$ (CDCl_3) δ : 1.29 (quint, $J = 7.6$ Hz, 2H, CH_2), 1.54 (quint, $J = 7.6$ Hz, 2H, CH_2), 1.67 (quint, $J = 7.2$ Hz, 2H, CH_2), 2.63 (t, $J = 7.2$ Hz, 2H, $\text{CH}_2\text{C=O}$), 2.86 (s, 4H, NHS), 3.45 (d, $J = 6.8$ Hz, 2H, CH_2N), 6.75 (s, 2H, CH=CH).

(2,5-Dioxopyrrolidin-1-yl)-4-[(2,5-dioxopyrrol-1-yl)methyl]cyclohexanecarboxylate (SMCC) (6). Yield 0.89 g (89%). $^1\text{H-NMR}$ spectrum corresponds to the literature data [85,87]. $^1\text{H-NMR}$ (CDCl_3) δ : 1.01–1.14 (m, 2H, cyclohexyl CH_2^{ax}), 1.47–1.61 (m, 2H, cyclohexyl $\text{COCHCH}_2^{\text{ax}}$), 1.60–1.75 (m, 1H, cyclohexyl CH), 1.76–1.85 (m, 2H, cyclohexyl CH_2^{eq}), 2.11–2.22 (m, 2H, cyclohexyl $\text{COCHCH}_2^{\text{eq}}$), 2.55–2.64 (m, 1H, cyclohexyl COCH), 2.83 (s, 4H, NHS), 3.40 (d, $J = 7.3$ Hz, 2H, CH_2N), 6.72 (s, 2H, CH=CH).

3.2.3. Synthesis of Conjugates of Aminobisphosphonic Acids with Maleimidosuccinimide Linkers 7–14

The synthesis described in [79] was modified. Bisphosphonates 1–3 (0.04 mmol) are dissolved in 0.6 mL of water, the pH of the solution is adjusted to 8–9 with 0.1 N NaOH solution (~150 μL). With good stirring, an equimolar amount of linker 4–6 (0.04 mmol) dissolved in 0.6 mL of acetone is added to the resulting solution. The reaction mass is stirred at room temperature for 15–30 min, then neutralized to pH = 7 with a 0.1 N HCl solution and concentrated under reduced pressure. Compounds 7–14 are obtained as white powders.

(3-[[3-(2,5-Dioxo-2,5-dihydro-1H-pyrrol-1-yl)propanoyl]amino]-1-hydroxypropane-1,1-diyl)-bis-(phosphonic acid) (BMPS- β) (7). Yield 0.009 g (60%). $^1\text{H-NMR}$ (D_2O): 1.93–2.09 (m, 2H, C^2H_2), 2.42 (t, $^3J = 6.5$ Hz, 2H, C^5H_2), 3.35 (t, $^3J = 7.8$ Hz, 2H, C^3H_2), 3.71 (t, $^3J = 6.0$ Hz, 2H, C^6H_2), 6.78 (s, HC=CH). $^{13}\text{C-NMR}$ (D_2O): 32.61 (C^2), 34.37 (C^6), 34.77 (C^5), 35.57 (t, $^3J_{\text{C-P}} = 7.8$ Hz, C^6), 72.87 (t, $^1J_{\text{C-P}} = 133.7$ Hz, C^1), 134.43 (C^8), 172.65 (C^4), 173.01 (C^7). $^{31}\text{P-NMR}$ (D_2O): 17.68. MALDI-TOF/TOF m/z 446.093 [$\text{M} + \text{Na} + \text{K}$] $^+$, 468.063 [$\text{M} + 2\text{Na} + \text{K}$] $^+$, calc. for $\text{C}_{10}\text{H}_{16}\text{N}_2\text{O}_{10}\text{P}_2$ 386.189.

(3-[[6-(2,5-Dioxo-2,5-dihydro-1H-pyrrol-1-yl)hexanoyl]amino]-1-hydroxypropane-1,1-diyl)-bis-(phosphonic acid) (EMCS- β) (8). (4-[[3-(2,5-Dioxo-2,5-dihydro-1H-pyrrol-1-yl)propanoyl]amino]-1-hydroxybutane-1,1-diyl) bis(phosphonic acid) (BMPS- γ) (9). Yield 0.014 g (88%). $^1\text{H-NMR}$ (D_2O): 1.63–1.76 (m, 2H, C^3H_2), 1.77–1.89 (m, 2H, C^2H_2), 2.42 (t, $^3J = 6.4$ Hz, 2H, C^6H_2), 3.06 (t, $^3J = 6.8$ Hz, 2H, C^4H_2), 3.71 (t, $^3J = 6.6$ Hz, 2H, C^7H_2), 6.78 (s, HC=CH). $^{13}\text{C-NMR}$ (D_2O): 23.18 (t, $^3J_{\text{C-P}} = 6.8$ Hz, C^3), 31.03 (C^2), 34.46 (C^6), 34.70 (C^7), 40.14 (C^4), 73.78 (t, $^1J_{\text{C-P}} = 134.8$ Hz, C^1), 134.47 (C^9), 172.66 (C^8), 173.37 (C^5). $^{31}\text{P-NMR}$ (D_2O): 18.20. MALDI-TOF/TOF m/z 400.080 [M] $^+$, calc. for $\text{C}_{11}\text{H}_{18}\text{N}_2\text{O}_{10}\text{P}_2$ 400.215.

(4-[[6-(2,5-Dioxo-2,5-dihydro-1H-pyrrol-1-yl)hexanoyl]amino]-1-hydroxybutane-1,1-diyl)bis(phosphonic acid) (EMCS- γ) (10). Yield 0.014 g (79%). $^1\text{H-NMR}$ (D_2O): 1.12–1.28 (m, 2H, C^8H_2), 1.41–1.58 (m, 4H, C^7H_2 , C^9H_2), 1.66–1.80 (m, 2H, C^3H_2), 1.80–1.95 (m, 2H, C^2H_2), 2.14 (t, $^3J = 7.5$ Hz, 2H, C^6H_2), 3.11 (t, $^3J = 6.8$ Hz, 2H, C^4H_2), 3.42 (t, $^3J = 6.9$ Hz, 2H, C^{10}H_2), 6.76 (s, 2H, HC=CH). $^{13}\text{C-NMR}$ (D_2O): 23.36 (C^3), 24.87 (C^7), 25.26 (C^8), 27.43 (C^9), 31.06 (C^2), 35.61 (C^6), 37.34 (C^{10}), 39.98 (C^4), 73.81 (t, $^1J_{\text{C-P}} = 134.1$ Hz, C^1), 134.26 (C^{12}), 173.41 (C^{11}), 176.80 (C^5). $^{31}\text{P-NMR}$ (D_2O): 18.21. MALDI-TOF/TOF m/z 440.322 [$\text{M} - 2\text{H}$] $^+$, calc. for $\text{C}_{14}\text{H}_{24}\text{N}_2\text{O}_{10}\text{P}_2$ 442.295.

(6-[[3-(2,5-Dioxo-2,5-dihydro-1H-pyrrol-1-yl)propanoyl]amino]-1-hydroxyhexane-1,1-diyl)bis(phosphonic acid) (BMPS- ϵ) (11). Yield 0.013 g (79%). $^1\text{H-NMR}$ (D_2O): 1.11–1.22 (m, 2H, C^4H_2), 1.32–1.43 (m, 2H, C^5H_2), 1.42–1.56 (m, 2H, C^3H_2), 1.76–1.91 (m, 2H, C^2H_2), 2.41 (t, $^3J = 6.0$ Hz, 2H, C^8H_2), 3.04 (t, $^3J = 6.8$ Hz, 2H, C^6H_2), 3.71 (t, $^3J = 6.4$ Hz, 2H, C^9H_2), 6.82 (s, 2H, C^{11}H_2), $^{13}\text{C-NMR}$ (D_2O): 23.23 (t, $^3J_{\text{C-P}} = 5.8$ Hz, C^3), 27.00 (C^4), 27.97 (C^5), 33.56 (C^2), 34.55 (C^9), 34.83 (C^8), 39.41 (C^6), 74.18 (s, $^1J_{\text{C-P}} = 134.5$ Hz, C^1), 134.53 (C^{11}), 172.60 (C^{10}), 173.21 (C^7). $^{31}\text{P-NMR}$ (D_2O): 18.50. MALDI-TOF/TOF m/z 428.086 [M] $^+$, calc. for $\text{C}_{13}\text{H}_{22}\text{N}_2\text{O}_{10}\text{P}_2$ 428.270.

(6-[[6-(2,5-Dioxo-2,5-dihydro-1H-pyrrol-1-yl)hexanoyl]amino]-1-hydroxyhexane-1,1-diyl)bis(phosphonic acid) (EMCS- ϵ) (12). Yield 0.014 g (75%). $^1\text{H-NMR}$ (D_2O): 1.13–1.21 (m, 2H, C^{10}H_2), 1.20–1.31 (m, 2H, C^4H_2), 1.38–1.52 (m, 2H, C^5H_2), 1.44–1.57 (m, 6H, C^3H_2 , C^9H_2 , C^{11}H_2), 1.78–1.92 (m, 2H, C^2H_2), 2.13 (t,

$^3J = 7.2$ Hz, 2H, C⁸H₂), 3.09 (t, $^3J = 6.7$ Hz, 2H, C⁶H₂), 3.42 (t, $^3J = 6.8$ Hz, 2H, C¹²H₂), 6.76 (s, 2H, C¹⁴H₂). ¹³C-NMR (D₂O): 23.23 (t, $^3J_{C-P} = 6.0$ Hz, C³), 24.90 (C⁹), 25.33 (C¹⁰), 26.92 (C⁴), 27.26 (C¹¹), 28.12 (C⁵), 33.55 (C²), 35.57 (C⁸), 37.46 (C¹²), 39.29 (C⁶), 74.21 (t, $^1J_{C-P} = 133.6$ Hz, C¹), 134.27 (C¹⁴), 173.41 (C¹³), 176.66 (C⁷). ³¹P-NMR (D₂O): 18.52. MALDI-TOF/TOF *m/z*: 470.391 [M]⁺, calc. for C₁₆H₂₈N₂O₁₀P₂ 470.348.

{4-[(4-[(2,5-Dioxo-2,5-dihydro-1H-pyrrol-1-yl)methyl]cyclohexyl)carbonyl]amino}-1-hydroxybutane-1,1-diyl} bis(phosphonic acid) (SMCC- γ) (**13**). Yield 0.017 g (93%). ¹H-NMR (D₂O): 0.86–1.00, 1.60–1.71 (m, 4H, C⁸H₂), 1.16–1.34, 1.71–1.81 (m, 4H, C⁷H₂), 1.48–1.65 (m, 1H, C⁹H), 1.64–1.78 (m, 2H, C³H₂), 1.80–1.92 (m, 2H, C²H₂), 2.06–2.16 (m, 1H, C⁶H), 3.10 (t, $^3J = 6.7$ Hz, 2H, C⁴H₂), 3.28 (d, $^3J = 7.0$ Hz, 2H, C¹⁰H₂), 6.75 (s, 2H, CH=CH). ¹³C-NMR (D₂O): 23.46 (t, $^3J_{C-P} = 6.2$ Hz, C³), 28.33 (C⁷), 29.14 (C⁸), 31.15 (C²), 36.05 (C⁹), 39.95 (C⁴), 43.47 (C¹⁰), 44.86 (C⁶), 73.83 (t, $^1J_{C-P} = 132.3$, C¹), 134.17 (C¹²), 173.58 (C¹¹), 179.68 (C⁵). ³¹P-NMR (D₂O): 18.25.

{6-[(4-[(2,5-Dioxo-2,5-dihydro-1H-pyrrol-1-yl)methyl]cyclohexyl)carbonyl]amino}-1-hydroxyhexane-1,1-diyl} bis(phosphonic acid) (SMCC- ϵ) (**14**). Yield 0.018 g (90%). ¹H-NMR (D₂O): 0.86–1.00, 1.61–1.70 (m, 4H, C¹⁰H₂), 1.20–1.30 (m, 2H, C⁴H₂), 1.23–1.34, 1.70–1.80 (m, 2H, C⁹H₂), 1.38–1.52 (m, 2H, C⁵H₂), 1.44–1.56 (m, 2H, C³H₂), 1.48–1.64 (m, 1H, C⁸H), 1.77–1.90 (m, 2H, C²H₂), 2.04–2.16 (m, 1H, C⁸H), 3.09 (t, $^3J = 6.8$ Hz, 2H, C⁶H₂), 3.28 (d, $^3J = 7.3$ Hz, 2H, C¹²H₂), 6.75 (s, 2H, CH=CH). ¹³C-NMR (D₂O): 23.40 (t, $^3J_{C-P} = 5.8$ Hz, C³), 26.90 (C⁴), 28.20 (C⁹), 28.34 (C⁵), 29.14 (C¹⁰), 33.73 (C²), 36.04 (C¹¹), 39.18 (C⁶), 43.46 (C¹²), 44.78 (C⁸), 74.26 (t, $^1J_{C-P} = 131.3$ Hz, C¹), 134.18 (C¹⁴), 173.58 (C¹³), 179.56 (C⁷). ³¹P-NMR (D₂O) 18.60. MALDI-TOF/TOF *m/z*: 499.066 [M + 3H]⁺, calc. for C₁₈H₃₀N₂O₁₀P₂ 496.137.

3.2.4. Synthesis of RGDC Derivatives 15–22

According to [79], 5 mg (0.01 mmol) of RGDC was dissolved in 1.45 mL of bidistilled water, the pH was adjusted to 7 by addition of 0.1 N NaOH (~120 μ L). An equivalent amount of compounds 7–14 (0.01 mmol) was added to the solution. The reaction mixture was stirred for 1–2 h at 38–40 °C until a pinkish-violet tint appeared, and then the solvent was removed under reduced pressure. Compounds 15–22 were obtained in quantitative yield as pink-white powders.

RGD-BMPS- β (**15**). ¹H-NMR (D₂O) δ : 1.55–1.68 (m, 2H, C²³H₂), 1.74–1.84 (m, 2H, C²²H₂), 1.96–2.10 (m, 2H, C²H₂), 2.38–2.45 (m, 2H, C⁵H₂), 2.52 (dd, $^3J = 8.4$ Hz, $^2J = 16.0$ Hz, 1H, C¹⁶HH), 2.66 (dd, $^3J = 4.9$ Hz, $^2J = 16.0$ Hz, 1H, C¹⁶HH), 2.94 (dd, $^3J = 8.5$ Hz, $^2J = 14.0$ Hz, 2H, C¹¹H₂), 3.11–3.20 (m, 3H, C²⁴H₂, C¹¹HH), 3.31–3.43 (m, 2H, C³H₂), 3.70 (t, $^3J = 7.0$ Hz, 2H, C⁶H₂), 3.70–3.80 (m, 1H, C²¹H), 3.87 (d, 1H, $^2J = 16.9$ Hz, C¹⁹HH), 4.02 (d, $^2J = 16.9$ Hz, 1H, C¹⁹HH), 4.40 (dd, $^3J = 4.1$ Hz, $^3J = 8.5$ Hz, 1H, C¹²H), 4.58–4.70 (m, 1H, C¹⁵H). ¹³C-NMR (D₂O): 23.77 (C²³), 29.49 (C²²), 32.97 (C²), 34.79 (C⁵), 35.84 (C⁶), 36.07 (C³), 38.21 (C¹⁶), 39.95 (C¹¹), 40.59 (C²⁴), 42.48 (C¹⁹), 51.39 (C¹⁵), 53.20 (C²¹), 54.39 (C¹²), 156.76 (C²⁵), 170.81 (C¹⁸), 172.54 (C¹⁴), 172.64 (C⁴), 173.82 (C²⁰), 176.43 (C¹³), 178.03 (C¹⁷), 178.91 (C⁷, C¹⁰). ³¹P-NMR (D₂O): 17.93. MALDI-TOF/TOF *m/z*: 836.169 [M + H]⁺, calc. for C₂₅H₄₃N₉O₁₇P₂S 835.671.

RGD-EMCS- β (**16**). NMR and mass spectrometry data correspond to those reported in [15].

RGD-BMPS- γ (**17**). ¹H-NMR (D₂O) δ : 1.58–1.70 (m, 2H, C²⁴H₂), 1.66–1.77 (m, 2H, C³H₂), 1.80–1.91 (m, 2H, C²H₂), 1.85–1.94 (m, 2H, C²³H₂), 2.40–2.46 (m, 2H, C⁶H₂), 2.62–2.84 (m, 2H, C¹⁷H₂), 2.98 (dd, $^3J = 8.3$ Hz, $^2J = 14.0$ Hz, 1H, C¹²HH), 3.01–3.12 (m, 2H, C⁴H₂), 3.10–3.20 (m, 1H, C¹²HH), 3.14–3.20 (m, 2H, C²⁵H₂), 3.68–3.75 (m, 2H, C⁷H₂), 3.85–3.97 (m, 1H, C²⁰HH), 3.98–4.08 (m, 2H, C²⁰HH), 3.99–4.09 (m, 1H, C²²H), 4.39–4.46 (m, 1H, C¹³H), 4.66–4.73 (m, 1H, C¹⁶H). ¹³C-NMR (D₂O): 23.22 (C³), 23.46 (C²⁴), 27.84 (C²³), 31.01 (C²), 33.62 (C⁶), 35.82 (C⁷), 36.60 (C¹⁷), 40.14 (C¹²), 40.32 (C⁴, C²⁵), 42.31 (C²⁰), 50.53 (C¹⁶), 52.82 (C²²), 54.21 (C¹³), 156.76 (C²⁶), 169.98 (C¹⁹), 172.01 (C¹⁵, C²¹), 172.89 (C⁵), 175.97 (C¹⁴), 176.14 (C¹⁸), 178.31 (C⁸, C¹¹). ³¹P-NMR (D₂O): 18.17. MALDI-TOF/TOF *m/z*: 849.15 [M]⁺, calc. for C₂₆H₄₅N₉O₁₇P₂S 849.698.

RGD-EMCS- γ (18). $^1\text{H-NMR}$ (D_2O) δ : 1.16–1.31 (m, 2H, C^8H_2), 1.38–1.55 (m, 4H, C^7H_2 , C^9H_2), 1.53–1.67 (m, 2H, C^{27}H_2), 1.61–1.77 (m, 2H, C^{26}H_2), 1.66–1.77 (m, 2H, C^3H_2), 1.77–1.90 (m, 2H, C^2H_2), 2.05–2.20 (m, 2H, C^6H_2), 2.52 (dd, $^3J = 8.4$ Hz, $^2J = 16.2$ Hz, 1H, C^{20}HH), 2.65 (dd, $^3J = 4.8$ Hz, $^2J = 16.2$ Hz, 1H, C^{20}HH), 2.93 (dd, $^3J = 8.5$ Hz, $^2J = 14.0$ Hz, 1H, C^{15}HH), 3.16 (dd, $^3J = 4.0$ Hz, $^2J = 14.0$ Hz, 1H, C^{15}HH), 3.08–3.15 (m, 2H, C^4H_2), 3.10–3.18 (m, 2H, C^{28}H_2), 3.42 (t, $^3J = 7.0$ Hz, 2H, C^{10}H_2), 3.54 (t, $^3J = 6.1$ Hz, 1H, C^{25}H), 3.86 (d, $^3J = 16.8$ Hz, 1H, C^{23}HH), 4.01 (d, $^3J = 16.8$ Hz, 1H, C^{23}HH), 4.40 (dd, $^3J = 4.0$ Hz, $^3J = 8.5$ Hz, 1H, C^{16}H), 4.59–4.68 (m, 1H, C^{19}H). $^{13}\text{C-NMR}$ (D_2O): 23.73 (C^3), 23.98 (C^{27}), 25.45 (C^8), 25.67 (C^7), 27.73 (C^9), 30.53 (C^{26}), 31.48 (C^2), 35.70 (C^6), 38.20 (C^{20}), 38.72 (C^{10}), 39.75 (C^4), 39.82 (C^{15}), 40.71 (C^{28}), 42.45 (C^{23}), 51.37 (C^{19}), 53.79 (C^{25}), 54.32 (C^{16}), 156.75 (C^{29}), 170.95 (C^{22}), 172.61 (C^{18}), 175.85 (C^{17}), 176.44 (C^{24}), 176.96 (C^5), 178.01 (C^{21}). $^{31}\text{P-NMR}$ (D_2O): 18.24. MALDI-TOF/TOF m/z : 910.533 [$\text{M} - 4\text{H} + \text{Na}$] $^+$, 926.498 [$\text{M} - 4\text{H} + \text{K}$] $^+$, calc. for $\text{C}_{29}\text{H}_{51}\text{N}_9\text{O}_{17}\text{P}_2\text{S}$ 891.778.

RGD-BMPS- ϵ (19). $^1\text{H-NMR}$ (D_2O) δ : 1.18–1.32 (m, 2H, C^4H_2), 1.38–1.46 (m, 2H, C^5H_2), 1.46–1.58 (m, 2H, C^3H_2), 1.57–1.72 (m, 2H, C^{26}H_2), 1.80–1.93 (m, 2H, C^2H_2), 1.84–1.96 (m, 2H, C^{25}H_2), 2.42 (t, $^3J = 6.7$ Hz, 2H, C^8H_2), 2.72–2.89 (m, 2H, C^{19}H_2), 2.94–3.02 (m, 1H, C^{14}HH), 3.00–3.10 (m, 2H, C^6H_2), 3.10–3.20 (m, 1H, C^{14}HH), 3.14–3.20 (m, 2H, C^{27}H_2), 3.67–3.75 (m, 2H, C^9H_2), 3.87–4.09 (m, 2H, C^{22}H_2), 3.98–4.08 (m, 1H, C^{24}H), 4.40–4.51 (m, 1H, C^{15}H), 4.65–4.77 (m, 1H, C^{18}H). $^{13}\text{C-NMR}$ (D_2O): 23.19 (C^3), 23.42 (C^{26}), 26.99 (C^4), 27.89 (C^5 , C^{25}), 33.58 (C^2), 33.71 (C^8), 35.75 (C^9), 35.93 (C^{19}), 39.50 (C^6 , C^{14}), 40.35 (C^{27}), 42.29 (C^{22}), 50.32 (C^{18}), 52.81 (C^{24}), 53.88 (C^{15}), 156.76 (C^{28}), 170.08 (C^{23}), 170.74 (C^{21}), 171.93 (C^{17}), 172.75 (C^7), 174.32 (C^{16}), 174.80 (C^{20}), 177.71 (C^{10} , C^{13}). $^{31}\text{P-NMR}$ (D_2O): 18.65. MALDI-TOF/TOF m/z : 879.242 [$\text{M} + 2\text{H}$] $^+$, calc. for $\text{C}_{28}\text{H}_{49}\text{N}_9\text{O}_{17}\text{P}_2\text{S}$ 877.751.

RGD-EMCS- ϵ (20). $^1\text{H-NMR}$ (D_2O) δ : 1.15–1.30 (m, 4H, C^4H_2 , C^{10}H_2), 1.41–1.53 (m, 2H, C^5H_2), 1.42–1.50 (m, 2H, C^3H_2), 1.45–1.61 (m, 4H, C^9H_2 , C^{11}H_2), 1.54–1.65 (m, 2H, C^{29}H_2), 1.64–1.74 (m, 2H, C^{28}H_2), 1.74–1.90 (m, 2H, C^2H_2), 2.13 (t, $^3J = 7.4$ Hz, 2H, C^8H_2), 2.48–2.72 (m, 2H, C^{22}H_2), 2.88–2.99 (m, 1H, C^{17}HH), 3.12–3.29 (m, 1H, C^{17}HH), 3.06–3.17 (m, 2H, C^6H_2), 3.10–3.18 (m, 2H, C^{30}H_2), 3.42 (t, $^3J = 7.10$ Hz, 2H, C^{12}H_2), 3.45–3.52 (m, 1H, C^{27}H), 3.82–3.92 (m, 1H, C^{25}HH), 3.93–4.04 (m, 1H, C^{25}HH), 4.40 (dd, $^3J = 4.0$ Hz, $^3J = 8.6$ Hz, 1H, C^{18}H), 4.56–4.72 (m, 1H, C^{21}H). $^{13}\text{C-NMR}$ (D_2O): 23.55 (t, $^3J_{\text{C-P}} = 6.0$ Hz, C^3), 24.03 (C^{29}), 25.48 (C^9), 26.15 (C^{10}), 26.36 (C^4 , C^{11}), 30.89 (C^{28}), 33.97 (C^2), 35.61 (C^8), 38.23 (C^{22}), 38.94 (C^{12}), 39.40 (C^6 , C^{17}), 40.72 (C^{30}), 42.40 (C^{25}), 51.43 (C^{21}), 53.93 (C^{27}), 54.64 (C^{18}), 74.37 (C^1), 156.74 (C^{31}), 171.03 (C^{24}), 172.61 (C^{20}), 177.92 (C^{23}), 176.46 (C^{19}), 176.56 (C^7 , C^{26}), 180.08 (C^{13} , C^{16}). $^{31}\text{P-NMR}$ (D_2O): 18.71. MALDI-TOF/TOF m/z : 920.398 [$\text{M} + \text{H}$] $^+$, calc. for $\text{C}_{31}\text{H}_{55}\text{N}_9\text{O}_{17}\text{P}_2\text{S}$ 919.831.

RGD-SMCC- γ (21). $^1\text{H-NMR}$ (D_2O) δ : 0.83–0.99 (m, 2H, C^8HH), 1.19–1.30 (m, 2H, C^7HH), 1.37–1.50 (m, 1H, C^9H), 1.52–1.65 (m, 2H, C^{27}H_2), 1.55–1.72 (m, 2H, C^{26}H_2), 1.67–1.77 (m, 2H, C^3H_2), 1.68–1.77 (m, 2H, C^8HH), 1.77–1.85 (m, 2H, C^7HH), 1.78–1.87 (m, 2H, C^2H_2), 1.96–2.06 (m, 1H, C^6H), 2.53 (dd, $^3J = 8.2$ Hz, $^2J = 16.0$ Hz, 1H, C^{22}HH), 2.66 (dd, $^3J = 4.8$ Hz, $^2J = 16.0$ Hz, 1H, C^{22}HH), 2.99–3.05 (m, 2H, C^{10}H_2), 2.93 (dd, $^3J = 8.6$ Hz, $^2J = 14.0$ Hz, 1H, C^{15}HH), 3.17 (dd, $^3J = 4.1$ Hz, $^2J = 14.0$ Hz, 1H, C^{15}HH), 3.08–3.12 (m, 2H, C^4H_2), 3.11–3.16 (m, 2H, C^{28}H_2), 3.41 (t, $^3J = 6.0$ Hz, 1H, C^{25}H), 3.85 (d, $^2J = 16.8$ Hz, 1H, C^{23}HH), 4.00 (d, $^2J = 16.8$ Hz, 1H, C^{23}HH), 4.40 (dd, $^3J = 4.1$ Hz, $^3J = 8.6$ Hz, 1H, C^{16}H), 4.63 (dd, $^3J = 4.8$ Hz, $^3J = 8.2$ Hz, 1H, C^{19}H). $^{13}\text{C-NMR}$ (D_2O): 23.86 (C^3), 24.13 (C^{27}), 29.25 (C^7), 29.53 (C^8), 29.56 (C^2), 31.25 (C^{26}), 36.71 (C^9), 38.27 (C^{20}), 39.71 (C^{15}), 40.17 (C^4), 40.83 (C^{28}), 42.45 (C^{23}), 45.41 (C^{10}), 46.98 (C^6), 51.36 (C^{19}), 54.06 (C^{25}), 54.32 (C^{16}), 156.74 (C^{29}), 171.11 (C^{22}), 172.63 (C^{18}), 176.49 (C^{17}), 177.91 (C^{21}), 178.01 (C^{24}). MALDI-TOF/TOF m/z : 941.786 [$\text{M} + \text{H} + \text{Na}$] $^+$, calc. for $\text{C}_{31}\text{H}_{53}\text{N}_9\text{O}_{17}\text{P}_2\text{S}$ 917.275.

RGD-SMCC- ϵ (22). $^1\text{H-NMR}$ (D_2O) δ : 0.84–1.00 (m, 2H, C^{10}HH), 1.18–1.32 (m, 2H, C^9HH), 1.20–1.30 (m, 2H, C^4H_2), 1.37–1.52 (m, 1H, C^{11}H), 1.41–1.52 (m, 2H, C^5H_2), 1.48–1.56 (m, 2H, C^3H_2), 1.55–1.66 (m, 2H, C^{29}H_2), 1.66–1.80 (m, 2H, C^{10}HH), 1.66–1.82 (m, 2H, C^{28}H_2), 1.79–1.85 (m, 2H, C^9HH), 1.77–1.87 (m, 2H, C^2H_2), 1.96–2.06 (m, 1H, C^8H), 2.53 (dd, $^3J = 8.4$ Hz, $^2J = 16.0$ Hz, 1H, C^{22}HH), 2.67 (dd, $^3J = 5.0$ Hz, $^2J = 16.0$ Hz, 1H, C^{22}HH), 2.99–3.05 (m, 2H, C^{12}H_2), 2.94 (dd, $^3J = 8.5$ Hz, $^2J = 14.0$ Hz, 1H, C^{17}HH), 3.18 (dd, $^3J = 4.1$ Hz, $^2J = 14.0$ Hz, 1H, C^{17}HH), 3.10 (t, $^3J = 6.7$ Hz, 2H, C^6H_2), 3.13–3.19 (m, 2H, C^{30}H_2), 3.58–3.66 (m, 1H, C^{27}H), 3.87 (d, $^2J = 16.9$ Hz, 1H, C^{25}HH), 4.02 (d, $^2J = 16.9$ Hz, 1H, C^{25}HH), 4.41 (dd,

$^3J = 4.1$ Hz, $^3J = 8.5$ Hz, 1H, C¹⁸H), 4.64 (dd, $^3J = 50$ Hz, $^3J = 8.4$ Hz, 1H, C²¹H). ¹³C-NMR (D₂O): 23.61 (C³), 23.92 (C²⁹), 27.01 (C⁴), 28.29 (C⁵), 29.26 (C⁹), 29.54 (C¹⁰), 30.19 (C²⁸), 34.22 (C²), 36.77 (C¹¹), 38.25 (C²²), 39.26 (C⁶), 39.86 (C¹⁷), 40.69 (C³⁰), 42.48 (C²⁵), 45.45 (C¹²), 46.92 (C⁸), 51.38 (C²¹), 53.67 (C²⁷), 54.36 (C¹⁸), 156.75 (C³¹), 172.59 (C²⁰), 175.44 (C²⁶), 176.46 (C¹⁹), 178.03 (C²³), 179.85 (C⁷). ³¹P-NMR (D₂O): 18.77.

3.3. Metal Sample Preparation and PEO Coating

The metal samples 10 mm in diameter were cut using a wire-EDM out of a commercially pure Cp-Ti sheet, 0.5 mm thick. Further, the disk samples were polished on a SiC grit to achieve the surface roughness $R_a < 0.1$ μm . Before the plasma electrolytic oxidation, the samples were washed with deionized water and ultrasonically cleaned in isopropanol for 5 min. To achieve a good contact both for the PEO and consequent electrochemical tests, a copper wire was attached into a small hole drilled at the sample edge. The contact place and the copper wire were coated with an epoxy resin which could withstand the electrochemical treatments. In order to produce the samples for the in vitro tests, a titanium screw holder was used to supply current to the sample. The holder was PEO coated to form a dielectric layer over its surface except the contact points prior to the treatment of the samples.

The plasma electrolytic oxidation was processed in a 10-L glass vessel equipped with a stainless steel heat exchanger arranged around its walls inside the electrolyte which comprised 20 g/L aqueous solution of Na₃PO₄·12H₂O of puris grade. The electrolyte temperature was maintained at 20 ± 1 °C using microcontroller regulation. The PEO process was run in a pulsed bipolar mode under the voltage regulation; the positive pulse was 470 V, negative 40 V; the frequency was 300 Hz. The positive pulse duration was 1.7 ms, the negative pulse was 0.87 ms; both separated with pauses of 0.38 ms. The PEO treatment duration was 5 min.

3.4. Surface Characterization

The PEO coating was studied using a JSM-6490LV scanning electron microscope (JEOL, Tokyo, Japan) at accelerating voltage of 10 kV. Both top view and cross-sections were examined. The coating thickness was measured using a Positector 6000 eddy current gauge (Defelsko, Ogdensburg, NY, USA) of N-type. The surface roughness was measured with TR-220 profilometer. In order to evaluate the coating porosity, the SEM images were processed using ImageJ software using the technique described elsewhere [88]. By adjusting the threshold in the grayscale images, the relative surface area taken by the objects of interest being darker than the neighboring places was calculated by the program in percents. The phase composition of the surface layer was characterised by an Ultima IV X-ray diffractometer (Rigaku, Tokyo, Japan) in Cu K α radiation at 40 kV and 40 mA using 0.02 deg. step scan with 2 s exposure, from 20 to 80 degrees 2θ . Further, the XRD spectra were processed using the X'Pert Highscore Plus software (Philips) with PDF2 pattern database and a built-in SemiQuant algorithm was employed to quantify the amounts of the crystalline phases in the coating.

XPS spectra were obtained using a JEOL JPS 9010MX spectrometer equipped with an (Mg K α) X-ray source. The pressure in the analytical chamber during the spectral acquisition was less than 7×10^{-8} Pa. The survey spectra were collected from 0 to 1000 eV with a pass energy of 50 eV, and high-resolution spectra were collected for each detected element of interest (C, N, O, P, S, and Ti) with a pass energy of 10 eV. The JEOL SpecSurf Program V. 1.9.2 was used to identify the characteristic peaks, to calculate the elemental compositions, and to fit the peaks of the high-resolution spectra.

3.5. Electrochemical Tests

The electrochemical tests were carried out in Ringer's solution (0.86 wt% NaCl, 0.03 wt% KCl, 0.033 wt% CaCl₂, pH 7.4) at temperature 37.0 ± 0.2 °C using a P-5X electrochemical system (Elins, Moscow, Russia). After the open circuit potential (OCP) was settled within ± 20 mV for at least 30 min, the potentiodynamic polarization (PDP) test was run from -350 mV to $+350$ mV with respect to the settled OCP at a rate of 0.25 mV/s. The reference electrode was a silver chloride electrode filled with

3.5M KCl. The counter electrode was a platinum rod. The PDP results were processed using Tafel analysis [89]. For the PDP curves having linear Tafel regions at ± 200 mV overpotentials, both anodic and cathodic slopes were used; for those having only cathodic linear Tafel regions, only cathodic slopes were used. The corrosion current i_{corr} was evaluated at the intersection of cathodic and anodic (if available) tangent lines with the level of E_{corr} . The polarization resistance R_p was evaluated as a slope of the polarization curve at ± 10 mV overpotentials for all the samples [90].

3.6. In Vitro Assessment

The PEO coated Ti samples were ultrasonically cleaned for 10 min in 95% ethanol and finally washed with deionized water, dried on air and sterilized by autoclaving at 134 °C. This temperature does not affect the PEO coating. In order to deposit the organic pore filler, the PEO coated Ti samples were put into a Petri dish with 10^{-3} M solutions of the RGD-derivatives, which were preliminarily sterilized by filtration with CA 0.22 μm filter. In 1 h the samples were dried on air in a laminar box. Then, all the samples were put into a plastic 24-well tissue culture plate.

Human embryonic lung fibroblasts (FLECH-104) and mesenchymal stem cells of human fat tissue (MSC) were purchased from BIOLOT (Saint Petersburg, Russia), human osteosarcoma cells (MG-63) were obtained from Russian cellular collection, Institute of Cytology RAS (Saint Petersburg, Russia). The cells were cultured in Dulbecco's modified Eagle's medium (DMEM) (Sigma) containing 10% fetal bovine serum (FBS) (BioWest) and gentamicin, in 25-cm² culture flasks (SPL life Sciences, Pocheon-si, South Korea) in a humidified 5% CO₂ atmosphere. The medium was changed twice a week. After reaching a monolayer, the cells were detached using 0.25% trypsin solution (PanEco, Moscow, Russia) and counted using automated cell counter TC20 (BioRad, Hercules, CA, USA).

The FLECH-104, MSC or MG-63 cells suspension was placed into each well of the plate with the samples (0.8 mL containing $20 \cdot 10^3$ cells). The cells in the wells with uncoated Ti+PEO samples were treated as a control. The culture plates were incubated for 7 days in the standard conditions (37 °C, 5 vol% CO₂). The culture plate itself (polystyrene) was used as a blank.

The cell proliferation was determined by EZ4U assay (Biomedica, Vienna, Austria), a modification of MTT test, which evaluates the cell metabolic activity is proportional to the number of adherent cells. Three samples of each type were transferred after the incubation into another 24-well plate with 0.8 mL of fresh DMEM medium. Then 80 μL of activated EZ4U solution was added to every well and incubated at 37 °C, 5 vol% CO₂ for 3.5 h. Optical absorbance was measured using microplate reader (Spark10M, Tecan, Männedorf, Switzerland) at 450 nm with a reference wavelength of 620 nm. The optical density per mm² was calculated as:

$$\text{OD}(\%) = \frac{(a - a_{\text{blank}})}{(A - a_{\text{blank}})} \cdot 100\% \quad (1)$$

where a —absorbance of the test sample at 450 nm minus absorbance at 620 nm; A —absorbance of the control sample at 450 nm minus absorbance at 620 nm; a_{blank} —the absorbance of the blank solution of DMEM with no cells at 450 nm and at 620 nm.

The mean value and the standard deviation for four measurements of the optical density were calculated with respect to the control.

4. Conclusions

We have synthesized a set of RGD-derivatives of amino bisphosphonates, obtained from β -alanine, γ -aminobutyric and ϵ -aminocaproic acids, containing various linkers (BMPS, EMSC, SMCC) and used them as organic top coatings on porous PEO layer on titanium. The compounds can be introduced into the PEO coating pores due to the presence of bisphosphonate groups that facilitate physicochemical adsorption. Electrochemical studies showed that after RGD functionalization, the PEO surface gets slightly nobler, but the corrosion currents notably increase; also, the anodic PDP curves of the PEO surface lose the passivation region after the introduction of the RGD-derivatives, so their presence

can be assessed by indirect electrochemical tests. The presence of organic molecules in the coating was confirmed by XPS spectroscopy. The appearance of compounds 15–20 on the surface provided a decrease in the Ti 2p line intensity and an increase of N1s and C1s line intensities; in addition, a significant decrease in the ratio of Ti 2p/C 1s and Ti 2p/P 2p was observed.

In vitro studies on proliferation and viability of fibroblasts, mesenchymal stem cells and osteoblast-like cells showed the dependence of the molecule bioactivity on the structure of the anchor and linker. In particular, RGD derivatives with relatively short bisphosphonate anchors and BMPS linker, as well as molecules containing a linker with a cyclohexyl fragment, increase cell proliferation on the surface of PEO-modified titanium. RGDC without anchor on Ti-PEO does not affect the cell proliferation. RGD-functionalized β -BMPS, γ -BMPS, γ -SMCC, ε -SMCC can be recommended as promising candidates for further in vivo research.

Supplementary Materials: The following are available online. Figures S1–S27: NMR and mass-spectra of compounds 1–22, Figure S28: XPS spectra of Ti-PEO modified by compounds 15–20.

Author Contributions: Conceptualization, L.V.P., and E.V.P.; investigation, E.S.L., Z.R.G., G.U.G., V.R.M., R.G.F., K.V.D., and G.S.D.; writing—original draft preparation, L.V.P.; writing—review and editing, E.V.P.; supervision, L.V.P. and E.V.P.; project administration, E.S.L. All authors have read and agreed to the published version of the manuscript.

Funding: The authors are grateful to the financial support received through RFBR project No. 17-03-01042. The part of the research was carried out in accordance with federal program № AAAA-A19-119022290012-3.

Acknowledgments: The structural studies of compounds (1)–(22) were carried out at the Center for Collective Use “Agidel” at the Institute of Petrochemistry and Catalysis, Russian Academy of Sciences. The authors also thank Nanotech Centre at Ufa State Aviation Technical University for the surface characterisation.

Conflicts of Interest: The authors declare no conflict of interest. The funders had no role in the design of the study; in the collection, analyses, or interpretation of data; in the writing of the manuscript, or in the decision to publish the results.

References

1. Wu, S.; Liu, X.; Yeung, K.W.K.; Liu, C.; Yang, X. Biomimetic porous scaffolds for bone tissue engineering. *Mater. Sci. Eng. R Rep.* **2014**, *80*, 1–36. [[CrossRef](#)]
2. Geetha, M.; Singh, A.K.; Asokamani, R.; Gogia, A.K. Ti based biomaterials, the ultimate choice for orthopaedic implants—A review. *Prog. Mater. Sci.* **2009**, *54*, 397–425. [[CrossRef](#)]
3. Mohedano, M.; Guzman, R.; Arrabal, R.; López Lacomba, J.L.; Matykina, E. Bioactive plasma electrolytic oxidation coatings—The role of the composition, microstructure, and electrochemical stability. *J. Biomed. Mater. Res. Part B Appl. Biomater.* **2013**, *101*, 1524–1537. [[CrossRef](#)] [[PubMed](#)]
4. Cordeiro, J.M.; Nagay, B.E.; Ribeiro, A.L.R.; da Cruz, N.C.; Rangel, E.C.; Fais, L.M.G.; Vaz, L.G.; Barão, V.A.R. Functionalization of an experimental Ti-Nb-Zr-Ta alloy with a biomimetic coating produced by plasma electrolytic oxidation. *J. Alloy. Compd.* **2019**, *770*, 1038–1048. [[CrossRef](#)]
5. Sharifi, H.; Aliofkhaezrai, M.; Darband, G.B.; Shrestha, S. A review on adhesion strength of peo coatings by scratch test method. *Surf. Rev. Lett.* **2018**, *25*. [[CrossRef](#)]
6. Qadir, M.; Li, Y.; Munir, K.; Wen, C. Calcium phosphate-based composite coating by micro-arc oxidation (MAO) for biomedical application: A review. *Crit. Rev. Solid State Mater. Sci.* **2018**, *43*, 392–416. [[CrossRef](#)]
7. Anderson, J.M. Biological responses to materials. *Ann. Rev. Mater. Sci.* **2001**, *31*, 81–110. [[CrossRef](#)]
8. Shekaran, A.; García, A.J. Extracellular matrix-mimetic adhesive biomaterials for bone repair. *J. Biomed. Mater. Res. Part A* **2011**, *96A*, 261–272. [[CrossRef](#)]
9. Meyers, S.R.; Grinstaff, M.W. Biocompatible and bioactive surface modifications for prolonged in vivo efficacy. *Chem. Rev.* **2012**, *112*, 1615–1632. [[CrossRef](#)]
10. Tejero, R.; Anitua, E.; Orive, G. Toward the biomimetic implant surface: Biopolymers on titanium-based implants for bone regeneration. *Prog. Polym. Sci.* **2014**, *39*, 1406–1447. [[CrossRef](#)]
11. Mas-Moruno, C. 3-Surface functionalization of biomaterials for bone tissue regeneration and repair. In *Peptides and Proteins as Biomaterials for Tissue Regeneration and Repair*; Barbosa, M.A., Martins, M.C.L., Eds.; Woodhead Publishing: Amsterdam, The Netherlands, 2018.

12. Park, J.M.; Koak, J.Y.; Jang, J.H.; Han, C.H.; Kim, S.K.; Heo, S.J. Osseointegration of anodized titanium implants coated with fibroblast growth factor-fibronectin (FGF-FN) fusion protein. *Int. J. Oral Maxillofac. Implant.* **2006**, *21*, 859–866.
13. Kazek-Kęsik, A.; Jaworska, J.; Krok-Borkowicz, M.; Gołda-Cępa, M.; Pastusiak, M.; Brzychczy-Włoch, M.; Pamuła, E.; Kotarba, A.; Simka, W. Hybrid oxide-polymer layer formed on Ti-15Mo alloy surface enhancing antibacterial and osseointegration functions. *Surf. Coat. Technol.* **2016**, *302*, 158–165. [[CrossRef](#)]
14. Zaporozhets, T.S.; Puz', A.V.; Sinebryukhov, S.L.; Gnednikov, S.V.; Smolina, T.P.; Besednova, N.N. Biocompatibility of modified osteoinductive calcium-phosphate coatings of metal implants. *Bull. Exp. Biol. Med.* **2017**, *162*, 366–369. [[CrossRef](#)] [[PubMed](#)]
15. Parfenov, E.V.; Parfenova, L.V.; Dyakonov, G.S.; Danilko, K.V.; Mukaeva, V.R.; Farrakhov, R.G.; Lukina, E.S.; Valiev, R.Z. Surface functionalization via PEO coating and RGD peptide for nanostructured titanium implants and their in vitro assessment. *Surf. Coat. Technol.* **2019**, *357*, 669–683. [[CrossRef](#)]
16. Ruoslahti, E. RGD and other recognition sequences for integrins. *Annu. Rev. Cell Dev. Biol.* **1996**, *12*, 697–715. [[CrossRef](#)] [[PubMed](#)]
17. Xiao, S.J.; Textor, M.; Spencer, N.D.; Wieland, M.; Keller, B.; Sigrist, H. Immobilization of the cell-adhesive peptide Arg–Gly–Asp–Cys (RGDC) on titanium surfaces by covalent chemical attachment. *J. Mater. Sci. Mater. Med.* **1997**, *8*, 867–872. [[CrossRef](#)]
18. Rezaia, A.; Johnson, R.; Lefkow, A.R.; Healy, K.E. Bioactivation of metal oxide surfaces. 1. surface characterization and cell response. *Langmuir* **1999**, *15*, 6931–6939. [[CrossRef](#)]
19. Zreiqat, H.; Akin, F.; Howlett, C.; Markovic, B.; Haynes, D.; Lateef, S.; Hanley, L. Differentiation of human bone-derived cells grown on GRGDSP-peptide bound titanium surfaces. *J. Biomed. Mater. Res.* **2003**, *64*, 105–113. [[CrossRef](#)]
20. Barber, T.A.; Gamble, L.J.; Castner, D.G.; Healy, K.E. In vitro characterisation of peptide-modified p(AAm-co-EG/AAc) IPN-coated titanium implants. *J. Orthop. Res.* **2006**, *24*, 1366–1376. [[CrossRef](#)]
21. Barber, T.A.; Golledge, S.L.; Castner, D.G.; Healy, K.E. Peptide-modified p(AAm-co-EG/AAc) IPNs grafted to bulk titanium modulate osteoblast behavior in vitro. *J. Biomed. Mater. Res. Part A* **2003**, *64A*, 38–47. [[CrossRef](#)]
22. Gawalt, E.S.; Avaltroni, M.J.; Danahy, M.P.; Silverman, B.M.; Hanson, E.L.; Midwood, K.S.; Schwarzbauer, J.E.; Schwartz, J. Bonding organics to Ti alloys: Facilitating human osteoblast attachment and spreading on surgical implant materials. *Langmuir* **2003**, *19*, 200–204. [[CrossRef](#)]
23. Pallu, S.; Bourget, C.; Bareille, R.; Labrugère, C.; Dard, M.; Sewing, A.; Jonczyk, A.; Vernizeau, M.; Christine Durrieu, M.; Amédée-Vilamitjana, J. The effect of cyclo-DfKRG peptide immobilization on titanium on the adhesion and differentiation of human osteoprogenitor cells. *Biomaterials* **2005**, *26*, 6932–6940. [[CrossRef](#)] [[PubMed](#)]
24. Bagno, A.; Piovan, A.; Dettin, M.; Chiarion, A.; Brun, P.; Gambaretto, R.; Fontana, G.; Di Bello, C.; Palu, G.; Castagliuolo, I. Human osteoblast-like cell adhesion on titanium substrates covalently functionalized with synthetic peptides. *Bone* **2007**, *40*, 693–699. [[CrossRef](#)] [[PubMed](#)]
25. Secchi, A.G.; Grigoriou, V.; Shapiro, I.M.; Cavalcanti-Adam, E.A.; Composto, R.J.; Ducheyne, P.; Adams, C.S. RGDS peptides immobilized on titanium alloy stimulate bone cell attachment, differentiation and confer resistance to apoptosis. *J. Biomed. Mater. Res. Part A* **2007**, *83*, 577–584. [[CrossRef](#)]
26. Kaemmerer, P.; Heller, M.; Brieger, J.; Klein, M.; Al-Nawas, B.; Gabriel, M. Immobilisation of linear and cyclic RGD-peptides on titanium surfaces and their impact on endothelial cell adhesion and proliferation. *Eur. Cell Mater.* **2011**, *21*, 364–372. [[CrossRef](#)]
27. Ryu, J.-J.; Park, K.; Kim, H.-S.; Jeong, C.-M.; Huh, J.-B. Effects of anodized titanium with Arg–Gly–Asp (RGD) peptide immobilized via chemical grafting or physical adsorption on bone cell adhesion and differentiation. *Int. J. Oral Maxillofac. Implant.* **2013**, *28*, 963–972. [[CrossRef](#)]
28. Lin, W.; Junjian, C.; Chengzhi, C.; Lin, S.; Sa, L.; Li, R.; Yingjun, W. Multi-biofunctionalization of a titanium surface with a mixture of peptides to achieve excellent antimicrobial activity and biocompatibility. *J. Mater. Chem. B* **2015**, *3*, 30–33. [[CrossRef](#)]
29. Heller, M.; Kumar, V.; Pabst, A.; Brieger, J.; Al-Nawas, B.; Kaemmerer, P. Osseous response on linear and cyclic RGD-peptides immobilized on titanium surfaces in vitro and in vivo: RGD-peptides influence osseous healing. *J. Biomed. Mater. Res. Part A* **2018**, *106*, 419–427. [[CrossRef](#)]

30. Ortiz-Hernandez, M.; Rappe, S.K.; Molmeneu, M.; Mas-Moruno, C.; Guillem-Marti, J.; Punset, M.; Caparros, C.; Calero, J.; Franch, J.; Fernandez-Fairen, M.; et al. two different strategies to enhance osseointegration in porous titanium: Inorganic thermo-chemical treatment versus organic coating by peptide adsorption. *Int. J. Mol. Sci.* **2018**, *19*, 2574. [[CrossRef](#)]
31. Tosatti, S.; Schwartz, Z.; Campbell, C.T.; Cochran, D.L.; VandeVondele, S.; Hubbell, J.A.; Denzer, A.; Simpson, J.; Wieland, M.; Lohmann, C.; et al. RGD-containing peptide GCRGYGRGDSPG reduces enhancement of osteoblast differentiation by poly(L-lysine)-graft-poly(ethylene glycol)-coated titanium surfaces. *J. Biomed. Mater. Res.* **2004**, *68A*, 458–472. [[CrossRef](#)]
32. Maddikeri, R.R.; Tosatti, S.; Schuler, M.; Chessari, S.; Textor, M.; Richards, R.G.; Harris, L.G. Reduced medical infection related bacterial strains adhesion on bioactive RGD modified titanium surfaces: A first step toward cell selective surfaces. *J. Biomed. Mater. Res. Part A* **2008**, *84A*, 425–435. [[CrossRef](#)] [[PubMed](#)]
33. Petrie, T.; Raynor, J.E.; Reyes, C.D.; Burns, K.L.; Collard, D.M.; García, A. The effect of integrin-specific bioactive coatings on tissue healing and implant osseointegration. *Biomaterials* **2008**, *29*, 2849–2857. [[CrossRef](#)] [[PubMed](#)]
34. Bell, B.F.; Schuler, M.; Tosatti, S.; Textor, M.; Schwartz, Z.; Boyan, B. Osteoblast response to titanium surfaces functionalized with extracellular matrix peptide biomimetics. *Clin. Oral Implant. Res.* **2011**, *22*, 865–872. [[CrossRef](#)] [[PubMed](#)]
35. Schliephake, H.; Scharnweber, D.; Dard, M.; Roessler, S.; Sewing, A.; Meyer, J.; Hoogestraat, D. Effect of RGD peptide coating of titanium implants on periimplant bone formation in the alveolar crest. *Clin. Oral Implant. Res.* **2002**, *13*, 312–319. [[CrossRef](#)] [[PubMed](#)]
36. Rammelt, S.; Illert, T.; Bierbaum, S.; Scharnweber, D.; Zwipp, H.; Schneiders, W. Coating of titanium implants with collagen, RGD peptide and chondroitin sulfate. *Biomaterials* **2006**, *27*, 5561–5571. [[CrossRef](#)] [[PubMed](#)]
37. Chua, P.-H.; Neoh, K.-G.; Kang, E.-T.; Wang, W. Surface functionalization of titanium with hyaluronic acid/chitosan polyelectrolyte multilayers and RGD for promoting osteoblast functions and inhibiting bacterial adhesion. *Biomaterials* **2008**, *29*, 1412–1421. [[CrossRef](#)]
38. Huang, Y.; Luo, Q.; Li, X.; Zhang, F.; Zhao, S. Fabrication and in vitro evaluation of the collagen/hyaluronic acid PEM coating crosslinked with functionalized RGD peptide on titanium. *Acta Biomater.* **2012**, *8*, 866–877. [[CrossRef](#)]
39. Jin, C.; Ren, L.-F.; Ding, H.-Z.; Shi, G.-S.; Lin, H.-S.; Zhang, F. Enhanced attachment, proliferation, and differentiation of human gingival fibroblasts on titanium surface modified with biomolecules. *J. Biomed. Mater. Res. Part B Appl. Biomater.* **2012**, *100*, 2167–2177. [[CrossRef](#)]
40. Zhao, B.; Tian, W.; Feng, H.; Lee, I.-S.; Cui, F. Effects of RGD peptide grafting to titanium dental implants on the adhesion of human gingival fibroblasts and epithelial cells. *Curr. Appl. Phys.* **2005**, *5*, 407–410. [[CrossRef](#)]
41. Karaman, O.; Kelebek, S.; Demirci, E.A.; iBIŞ, F.; Ulu, M.; Ercan, U. Synergistic Effect of Cold Plasma Treatment and RGD Peptide Coating on Cell Proliferation over Titanium Surfaces. *Tissue Eng. Regen. Med.* **2017**, *15*, 13–24. [[CrossRef](#)]
42. Yamamichi, N.; Pugdee, K.; Chang, W.-J.; Lee, S.-A.; Yoshinari, M.; Hayakawa, T.; Abiko, Y. Gene expression monitoring in osteoblasts on fibronectin derived peptide coated titanium. *Dent. Mater. J.* **2008**, *27*, 744–750. [[CrossRef](#)] [[PubMed](#)]
43. Oya, K.; Tanaka, Y.; Saito, H.; Kurashima, K.; Nogi, K.; Tsutsumi, H.; Tsutsumi, Y.; Doi, H.; Nomura, N.; Hanawa, T. Calcification by MC3T3-E1 cells on RGD peptide immobilized on titanium through electrodeposited PEG. *Biomaterials* **2009**, *30*, 1281–1286. [[CrossRef](#)] [[PubMed](#)]
44. Park, J.-W.; Kurashima, K.; Tustusmi, Y.; An, C.-H.; Suh, J.-Y.; Doi, H.; Nomura, N.; Noda, K.; Hanawa, T. Bone healing of commercial oral implants with RGD immobilization through electrodeposited poly(ethylene glycol) in rabbit cancellous bone. *Acta Biomater.* **2011**, *7*, 3222–3229. [[CrossRef](#)] [[PubMed](#)]
45. Hoyos-Nogués, M.; Buxadera-Palomero, J.; Ginebra, M.-P.; Manero, J.M.; Gil, F.J.; Mas-Moruno, C. All-in-one trifunctional strategy: A cell adhesive, bacteriostatic and bactericidal coating for titanium implants. *Colloids Surf. B Biointerfaces* **2018**, *169*, 30–40. [[CrossRef](#)]
46. Okamoto, K.; Matsuura, T.; Hosokawa, R.; Akagawa, Y. RGD peptides regulate the specific adhesion scheme of osteoblasts to hydroxyapatite but not to titanium. *J. Dent. Res.* **1998**, *77*, 481–487. [[CrossRef](#)]
47. Ferris, D.M.; Moodie, G.D.; Dimond, P.M.; Giorani, C.W.D.; Ehrlich, M.G.; Valentini, R.F. RGD-coated titanium implants stimulate increased bone formation in vivo. *Biomaterials* **1999**, *20*, 2323–2331. [[CrossRef](#)]

48. Elmengaard, B.; Bechtold, J.E.; Soballe, K. In vivo study of the effect of RGD treatment on bone ongrowth on press-fit titanium alloy implants. *Biomaterials* **2005**, *26*, 3521–3526. [[CrossRef](#)]
49. Reyes, C.D.; Petrie, T.A.; Burns, K.L.; Schwartz, Z.; Garcia, A.J. Biomolecular surface coating to enhance orthopaedic tissue healing and integration. *Biomaterials* **2007**, *28*, 3228–3235. [[CrossRef](#)]
50. Pallu, S.; Fricain, J.C.; Bareille, R.; Bourget, C.; Dard, M.; Sewing, A.; Amédée, J. Cyclo-DfKRG Peptide Modulates In Vitro and In Vivo Behavior of Human Osteoprogenitor Cells on Titanium Alloys. *Acta Biomater.* **2009**, *5*, 3581–3592. [[CrossRef](#)]
51. Mas-Moruno, C.; Dorfner, P.; Manzenrieder, F.; Neubauer, S.; Reuning, U.; Burgkart, R.; Kessler, H. Behavior of primary human osteoblasts on trimmed and sandblasted Ti6Al4V surfaces functionalized with integrin $\alpha\beta 3$ -selective cyclic RGD peptides. *J. Biomed. Mater. Res. Part A* **2013**, *101A*, 87–97. [[CrossRef](#)]
52. Yuran, S.; Dolid, A.; Reches, M. Resisting bacteria and attracting cells: Spontaneous formation of a bifunctional peptide-based coating by on-surface assembly approach. *ACS Biomater. Sci. Eng.* **2018**, *4*, 4051–4061. [[CrossRef](#)]
53. Auernheimer, J.; Zukowski, D.; Dahmen, C.; Kantlehner, M.; Enderle, A.; Goodman, S.L.; Kessler, H. Titanium implant materials with improved biocompatibility through coating with phosphonate-anchored cyclic RGD peptides. *ChemBioChem* **2005**, *6*, 2034–2040. [[CrossRef](#)] [[PubMed](#)]
54. Zorn, G.; Gotman, I.; Gutmanas, E.Y.; Adadi, R.; Salitra, G.; Sukenik, C.N. Surface Modification of Ti45Nb Alloy with an Alkylphosphonic Acid Self-Assembled Monolayer. *Chem. Mater.* **2005**, *17*, 4218–4226. [[CrossRef](#)]
55. Bly, R.A.; Cao, Y.; Moore, W.A.; Soboyejo, W. Investigation of the effects of alkane phosphonic acid/RGD coatings on cell spreading and the interfacial strength between human osteosarcoma cells and Ti–6Al–4V. *Mater. Sci. Eng. C* **2007**, *27*, 83–89. [[CrossRef](#)]
56. Heijink, A.; Schwartz, J.; Zobitz, M.E.; Nicole Crowder, K.; Lutz, G.E.; Sibonga, J.D. Self-assembled monolayer films of phosphonates for bonding RGD to titanium. *Clin. Orthop. Relat. Res.* **2008**, *466*, 977–984. [[CrossRef](#)] [[PubMed](#)]
57. Guillou-Buffello, D.; Bareille, R.; Gindre, M.; Sewing, A.; Laugier, P.; Amédée, J. Additive Effect of RGD Coating to Functionalized Titanium Surfaces on Human Osteoprogenitor Cell Adhesion and Spreading. *Tissue Eng. Part A* **2008**, *14*, 1445–1455. [[CrossRef](#)] [[PubMed](#)]
58. Beuvelot, J.; Portet, D.; Lecollinet, G.; Moreau, M.F.; Baslé, M.F.; Chappard, D.; Libouban, H. In vitro kinetic study of growth and mineralization of osteoblast-like cells (Saos-2) on titanium surface coated with a RGD functionalized bisphosphonate. *J. Biomed. Mater. Res. Part B Appl. Biomater.* **2009**, *90B*, 873–881. [[CrossRef](#)]
59. Queffelec, C.; Petit, M.; Janvier, P.; Knight, D.A.; Bujoli, B. Surface modification using phosphonic acids and esters. *Chem. Rev.* **2012**, *112*, 3777–3807. [[CrossRef](#)]
60. Goura, J.; Chandrasekhar, V. Molecular metal phosphonates. *Chem. Rev.* **2015**, *115*, 6854–6965. [[CrossRef](#)]
61. Bujoli, B.; Queffelec, C. Fine-Tuning the Functionality of Inorganic Surfaces Using Phosphonate Chemistry. In *Tailored Organic-Inorganic Materials*; John Wiley & Sons: New York, NY, USA, 2015; pp. 299–318.
62. Gawalt, E.S.; Avaltroni, M.J.; Koch, N.; Schwartz, J. Self-assembly and bonding of alkanephosphonic acids on the native oxide surface of titanium. *Langmuir* **2001**, *17*, 5736–5738. [[CrossRef](#)]
63. Silverman, B.M.; Wiegand, K.A.; Schwartz, J. Comparative properties of siloxane vs. phosphonate monolayers on a key titanium alloy. *Langmuir* **2005**, *21*, 225–228. [[CrossRef](#)] [[PubMed](#)]
64. Portet, D.; Denizot, B.; Rump, E.; Lejeune, J.-J.; Jallet, P. nonpolymeric coatings of iron oxide colloids for biological use as magnetic resonance imaging contrast agents. *J. Colloid Interface Sci.* **2001**, *238*, 37–42. [[CrossRef](#)] [[PubMed](#)]
65. Lecollinet, G.; Delorme, N.; Edely, M.; Gibaud, A.; Bardeau, J.F.; Hindré, F.; Boury, F.; Portet, D. Self-assembled monolayers of bisphosphonates: Influence of side chain steric hindrance. *Langmuir* **2009**, *25*, 7828–7835. [[CrossRef](#)] [[PubMed](#)]
66. Yerokhin, A.L.; Nie, X.; Leyland, A.; Matthews, A.; Dowey, S.J. Plasma electrolysis for surface engineering. *Surf. Coat. Technol.* **1999**, *122*, 73–93. [[CrossRef](#)]
67. Han, Y.; Hong, S.H.; Xu, K. Structure and in vitro bioactivity of titania-based films by micro-arc oxidation. *Surf. Coat. Technol.* **2003**, *168*, 249–258. [[CrossRef](#)]
68. Walsh, F.C.; Low, C.T.J.; Wood, R.J.K.; Stevens, K.T.; Archer, J.; Poeton, A.R.; Ryder, A. Plasma electrolytic oxidation (PEO) for production of anodised coatings on lightweight metal (Al, Mg, Ti) alloys. *Trans. Inst. Met. Finish.* **2009**, *87*, 122–135. [[CrossRef](#)]

69. Jung, O.; Smeets, R.; Kopp, A.; Porchetta, D.; Hiester, P.; Heiland, M.; Friedrich, R.E.; Precht, C.; Hanken, H.; Gröbe, A.; et al. PEO-generated surfaces support attachment and growth of cells in vitro with no additional benefit for micro-roughness in Sa (0.2–4 μm). *In Vivo* **2016**, *30*, 27–33.
70. Parfenov, E.V.; Yerokhin, A.; Nevyantseva, R.R.; Gorbatkov, M.V.; Liang, C.J.; Matthews, A. Towards smart electrolytic plasma technologies: An overview of methodological approaches to process modelling. *Surf. Coat. Technol.* **2015**, *269*, 2–22. [[CrossRef](#)]
71. Yerokhin, A.; Parfenov, E.V.; Matthews, A. In situ impedance spectroscopy of the plasma electrolytic oxidation process for deposition of Ca- and P-containing coatings on Ti. *Surf. Coat. Technol.* **2016**, *301*, 54–62. [[CrossRef](#)]
72. Gnedenkov, S.V.; Sharkeev, Y.P.; Sinebryukhov, S.L.; Khrisanfova, O.A.; Legostaeva, E.V.; Zavidnaya, A.G.; Puz', A.V.; Khlusov, I.A.; Opra, D.P. Functional coatings formed on the titanium and magnesium alloys as implant materials by plasma electrolytic oxidation technology: Fundamental principles and synthesis conditions. *Corros Rev.* **2016**, *34*. [[CrossRef](#)]
73. Santos-Coquillat, A.; Gonzalez Tenorio, R.; Mohedano, M.; Martinez-Campos, E.; Arrabal, R.; Matykina, E. Tailoring of antibacterial and osteogenic properties of Ti6Al4V by plasma electrolytic oxidation. *Appl. Surf. Sci.* **2018**, *454*, 157–172. [[CrossRef](#)]
74. Uezono, M.; Takakuda, K.; Kikuchi, M.; Suzuki, S.; Moriyama, K. Hydroxyapatite/collagen nanocomposite-coated titanium rod for achieving rapid osseointegration onto bone surface. *J. Biomed. Mater. Res. Part B Appl. Biomater.* **2013**, *101*, 1031–1038. [[CrossRef](#)] [[PubMed](#)]
75. Kazemzadeh-Narbat, M.; Noordin, S.; Masri, B.A.; Garbuz, D.S.; Duncan, C.P.; Hancock, R.E.W.; Wang, R. Drug release and bone growth studies of antimicrobial peptide-loaded calcium phosphate coating on titanium. *J. Biomed. Mater. Res. Part B Appl. Biomater.* **2012**, *100 B*, 1344–1352. [[CrossRef](#)]
76. Gnedenkov, S.V.; Sinebryukhov, S.L.; Zavidnaya, A.G.; Egorkin, V.S.; Puz', A.V.; Mashtalyar, D.V.; Sergienko, V.I.; Yerokhin, A.L.; Matthews, A. Composite hydroxyapatite-PTFE coatings on Mg-Mn-Ce alloy for resorbable implant applications via a plasma electrolytic oxidation-based route. *J. Taiwan Inst. Chem. Eng.* **2014**, *45*, 3104–3109. [[CrossRef](#)]
77. Nielsen, O.; Buchardt, O. Facile Synthesis of Reagents Containing a Terminal Maleimido Ligand Linked to an Active Ester. *Synthesis* **1991**, *1991*, 819–821. [[CrossRef](#)]
78. Ede, N.J.; Tregear, G.W.; Haralambidis, J. Routine preparation of thiol oligonucleotides: Application to the synthesis of oligonucleotide-peptide hybrids. *Bioconjugate Chem.* **1994**, *5*, 373–378. [[CrossRef](#)]
79. Tyler, P.C.; Young, R.N.; Rodan, G.A.; Ruel, R. Prostaglandin Analog for Treating Osteoporosis. US Patent No. 5,409,911, 1995.
80. Moon, S.; Arrabal, R.; Matykina, E. 3-Dimensional structures of open-pores in PEO films on AZ31 Mg alloy. *Mater. Lett.* **2015**, *161*, 439–441. [[CrossRef](#)]
81. Diamanti, M.V.; Del Curto, B.; Pedferri, M. Anodic oxidation of titanium: From technical aspects to biomedical applications. *J. Appl. Biomater. Biomech.* **2011**, *9*, 55–69. [[CrossRef](#)]
82. Zorn, G.; Gotman, I.; Gutmanas, E.Y.; Adadi, R.; Sukenik, C.N. Surface modification of Ti45Nb alloy by immobilization of RGD peptide via self assembled monolayer. *J. Mater. Sci. Mater. Med.* **2007**, *18*, 1309–1315. [[CrossRef](#)]
83. Zoulalian, V.; Zürcher, S.; Tosatti, S.; Textor, M.; Monge, S.; Robin, J.J. Self-assembly of poly (ethylene glycol)-poly (alkyl phosphonate) terpolymers on titanium oxide surfaces: Synthesis, interface characterization, investigation of nonfouling properties, and long-term stability. *Langmuir* **2010**, *26*, 74–82. [[CrossRef](#)]
84. Kovács, R.; Grün, A.; Németh, O.; Garadnay, S.; Greiner, I.; Keglevich, G. The synthesis of pamidronic derivatives in different solvents: An optimization and a mechanistic study. *Heteroat. Chem.* **2014**, *25*, 186–193. [[CrossRef](#)]
85. Paterson, M.J.; Eggleston, I.M. Convenient preparation of N-maleoyl amino acid succinimido esters using N-trifluoroacetoxysuccinimide. *Synth. Commun.* **2008**, *38*, 303–308. [[CrossRef](#)]
86. Song, H.Y.; Ngai, M.H.; Song, Z.Y.; MacAry, P.A.; Hopley, J.; Lear, M.J. Practical synthesis of maleimides and coumarin-linked probes for protein and antibody labelling via reduction of native disulfides. *Org. Biomol. Chem.* **2009**, *7*, 3400–3406. [[CrossRef](#)] [[PubMed](#)]
87. Leonard, N.M.; Brunckova, J. One-pot synthesis of succinimidyl-4-(N-maleimidomethyl)cyclohexane-1-carboxylate (SMCC). *Org. Prep. Proced. Int.* **2012**, *44*, 180–183. [[CrossRef](#)]
88. Abràmoff, M.D.; Magalhães, P.J.; Ram, S.J. Image processing with imageJ. *Biophoton. Int.* **2004**, *11*, 36–41.

89. Chung, F.H. Quantitative interpretation of X-ray diffraction patterns of mixtures. I. Matrix-flushing method for quantitative multicomponent analysis. *J. Appl. Crystallogr.* **1974**, *7*, 519–525. [[CrossRef](#)]
90. Scully, J.R. Polarization resistance method for determination of instantaneous corrosion rates. *Corrosion* **2000**, *56*, 199–218. [[CrossRef](#)]

Sample Availability: Samples of the compounds are not available from the authors.



© 2020 by the authors. Licensee MDPI, Basel, Switzerland. This article is an open access article distributed under the terms and conditions of the Creative Commons Attribution (CC BY) license (<http://creativecommons.org/licenses/by/4.0/>).